



Mineralogy and geochemistry study of the Nyong River sediments, SW Cameroon: Implications for provenance, weathering, and tectonic setting

Yannick Steve Ngagoum Kontchipe¹ · Francis Temgo Sovie¹ · Gabriel Ngueutchoua² · Aristide Nadine Sonfack¹ · David Guimolaire Nkouathio¹ · Robinson Tchatchueng¹ · Gatien Romuald Kenfack Nguemo¹ · Théophile Njanko¹

Received: 8 February 2021 / Accepted: 22 April 2021 / Published online: 29 May 2021
© Saudi Society for Geosciences 2021

Abstract

Texture, mineralogy, heavy minerals, and major and trace elements, including REE, from surface sediment samples collected along the Nyong River (NR) were analyzed in the current study to characterize and discuss the intensity of weathering, provenance, and tectonic settings of the source area and estimate the chemical features that reflect the parental rocks, known from literature. The sediments are mainly fine- and coarse-grained sands, and the mineralogy is predominantly composed of quartz, accompanied by kaolinite, illite, opaque oxides, kyanite, rutile, zircon, tourmaline, sillimanite, garnet, and hypersthene. Geochemically, the sediments are classified as Fe–shale, Fe–sand, and quartz arenite. The CIA, PIA, CIW, and the A–CN–K and (A–K)–C–N plots indicate the high intensity of chemical weathering. The values of $\text{SiO}_2/\text{Al}_2\text{O}_3$, $\text{Al}_2\text{O}_3/\text{Na}_2\text{O}$, $\text{K}_2\text{O}/\text{Na}_2\text{O}$, ICV, and the ZTR index indicate the maturity of many samples. Most of the sediment samples experienced recycling, as revealed by the $\text{Al}_2\text{O}_3\text{--TiO}_2\text{--Zr}$ plot. Several bivariate plots such as Zr vs TiO_2 and Th/Co vs La/Sc, and the REE pattern and size of Eu, indicate derivation from a source area composed mostly of intermediate and felsic rocks and, in a lesser extent, of mafic source rocks. Tectonic discriminant diagrams based on major and trace elements indicate rift and passive margin settings, which is consistent with several tectonic history models of the Ntem complex and the Pan-African belt.

Keywords Nyong River · Ntem complex · Stream sediment · Provenance · Pan-African belt

Introduction

The geochemistry of clastic sediments is an important source of information in unraveling their provenance history (Cullers 2002; Saha et al. 2010; Ramos-Vázquez and Armstrong-Altrin 2019), the intensity of weathering (Roy et al. 2008; Gallala et al. 2009), and the tectonic setting of the source terrane (Armstrong-Altrin and Verma 2005; Sabaou et al. 2009). The recent clastic sediments, from nowadays river beds, are most suited for weathering and provenance studies

because they experienced minor or no post depositional processes, such as diagenesis and K-metasomatism (Ndjigui et al. 2015; Mbale Ngama et al. 2019). Furthermore, the spatial distribution of sediments in modern rivers is thought to be controlled mainly by the variations in the source areas (Nascimento et al. 2015), in spite of the fact that they are mixed by transport processes.

Previous provenance studies on the Atlantic equatorial area, which relied on the petrography, mineralogy and geochemistry, are very few (e.g., Ndjigui et al. 2015, 2018; Ekoa Bessa et al. 2018, 2020; Mbale Ngama et al. 2019; Mioumnde et al. 2019). Based on geochemistry of alluvial clay, Ndjigui et al. (2018) interpreted the provenance and depositional history of the Lokoundje River sediments. These sediments, which were deposited in an oxic environment, were derived from the basement of the watershed, which is made up of gneisses, amphibolites, migmatites, charnockites, and pyroxenites from the Nyong and Ntem units, located at the NW border of the Congo craton. Although these studies provide important constrains on the depositional milieu and

Responsible Editor: Domenico M. Doronzo

✉ Gabriel Ngueutchoua
ngueutchoua2@yahoo.fr

¹ Department of Earth Sciences, University of Dschang, P.O. Box: 67, Dschang, Cameroon

² Department of Earth Sciences, University of Yaoundé 1, P.O. Box: 812, Yaoundé, Cameroon

the source rock, stream sediments of many other drainage basins of this region, such as those of the Nyong River (NR) watershed, also made up of a wide range of rock types, are still to be investigated.

The geochemistry of the NR watershed sediments has not been documented yet. It is interesting to note that this river is located on the Atlantic equatorial area. In its upper reaches, it flows through the Pan-African Neoproterozoic belt. Towards the lower reaches, it encompasses the Ntem and Nyong units before entering the Atlantic sea. The tectonic framework of this basement terrane remains controversial due to poor constraints from geochemical and geochronological studies. The Pan-African belt presents all the features that characterize a collisional belt such as granulitic metamorphism and intensive plutonism associated with crustal melting. However, various and divergent tectonic models suggest either collision between the Congo craton and the mobile belt (Nzenti et al. 1984, 1988; Toteu et al. 2001) or collision between different blocks of the mobile belt (Toteu et al. 1991). Also, no clear evidence of oceanic rocks has yet been found and several workers suggest either a paleotectonic setting of an intracontinental extensional basin on the rifted northern margin of the Congo craton (Nzenti et al. 1984, 1988) or possibly a passive margin (Vicat and Pouclet 1995; Vicat et al. 1996; Feybesse et al. 1998; Pouclet et al. 2007). Regarding the provenance of the sediments and the tectonic setting of their source terranes, the alluviums from the NR provide an opportunity to study the effect of lithology change on sediment chemical composition, which has significance for the use of sediment chemistry as a proxy in interpretation of source region. On the other hand, the geochemistry of the NR sediments could lead, for the first time, to approximate the roles of some of the chemical and physical processes that control these deposits and evaluate their features that most closely mirror the nature of the watershed basement rocks, as described in the literature. This approach is based on the assumption that some immobile elements (e.g., La, Th) are more abundant in felsic than in basic rocks; therefore, their contents in sand-size sediments allow a distinction to be made between a felsic and a mafic source (Cullers et al. 1988). On the other hand, Bhatia (1983), Bhatia and Crook (1986), Roser and Korsch (1986, 1988), and Verma and Armstrong-Altrin et al. (2013, 2016) showed that plate tectonic processes impart a typical geochemical signature to sediment. Thus, different tectonic environments have distinctive provenance features and they are characterized by distinctive sedimentary processes.

In this study, the bulk sediment geochemistry and mineralogy of the NR sediments is reported. The aim of the current work is (1) to determine the geochemical variation among samples collected, (2) to deduce the potential variation in provenance signatures and source area weathering, and (3) to infer the tectonic setting of source rocks. Overall, this paper contributes to the knowledge of sedimentological

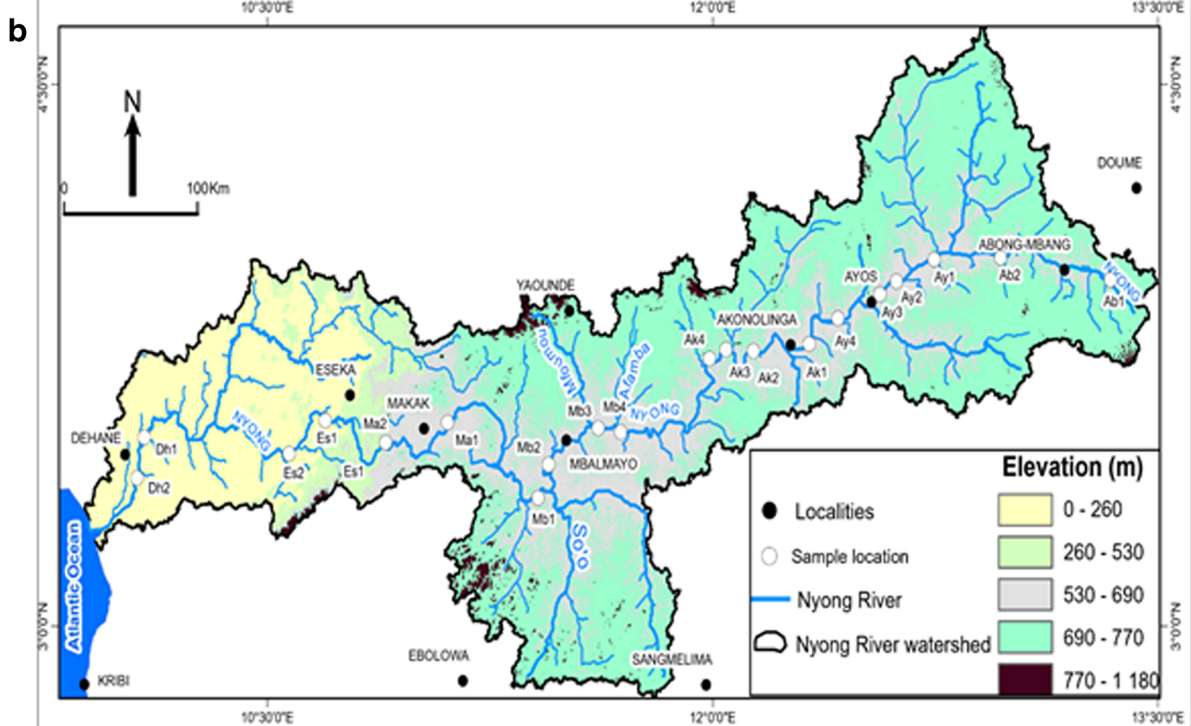
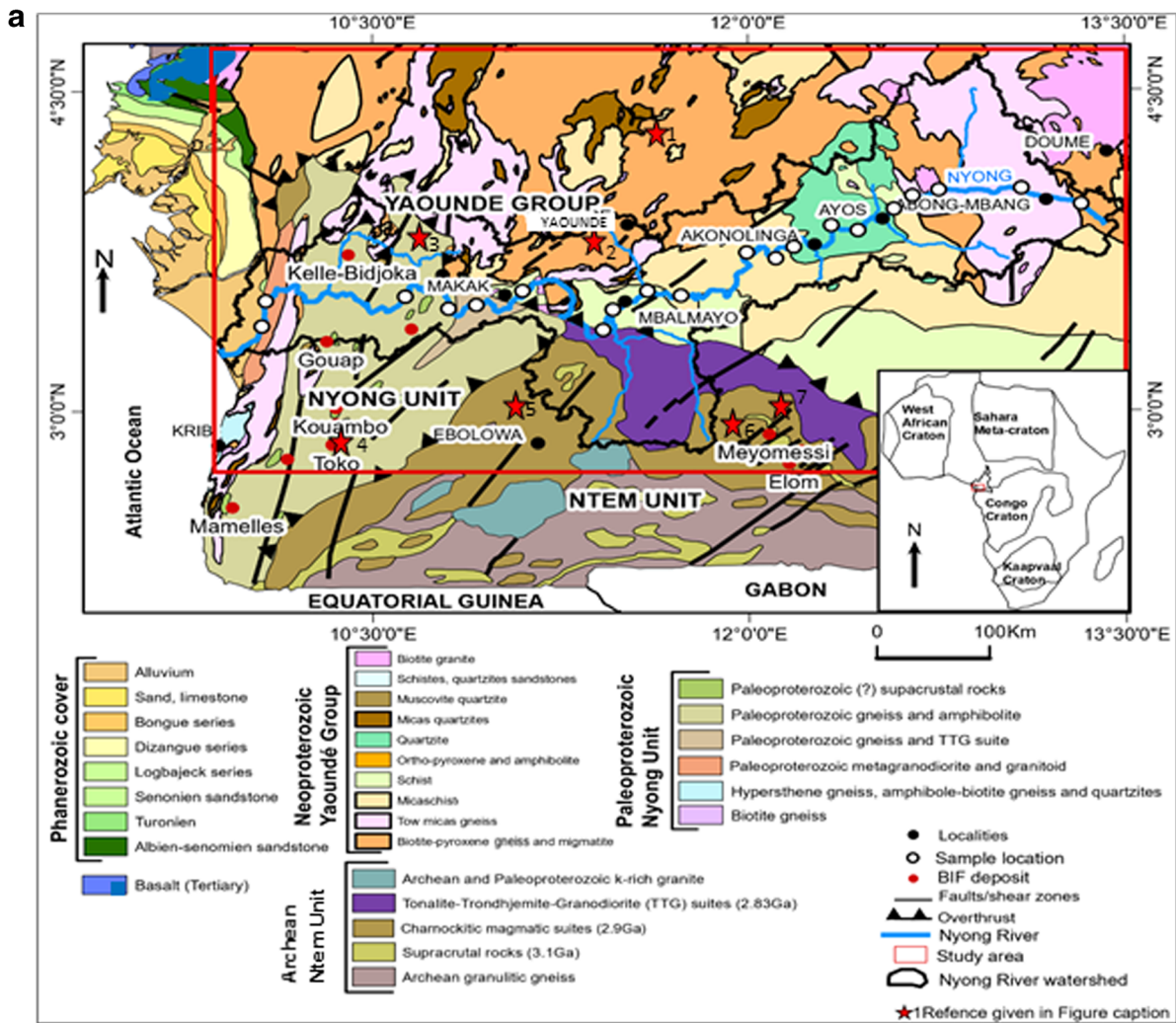
characteristics of stream sediments from the Nyong drainage basin, situated under warm and humid climate in the Atlantic equatorial region, and whose basement is made up of various Archean, Paleoproterozoic, and Neoproterozoic rocks.

Geographical and geological context

The NR drainage basin (9° 54′–13° 30′ E, 2° 48′–4° 32′ N; 27,800 km²; Olivry 1986) is located in a morphological unit called “the Southern Cameroonian Plateau,” which is a vast smoothly undulating surface, with elevation between 650 and 850 m (Fig. 1a, b). This area is covered by the equatorial **rain (evergreen) forest**. The NR (690 km of length) is the second major river, after the Sanaga River, draining along the said plateau and the southwestern Cameroonian coastal region. It has its headwaters towards the eastern part of the above Cameroonian plateau, near the locality of Abong Mbang, in the northern part of the equatorial **rain forest** (Olivry 1986). It follows a westerly direction with a slope gradient of 0.2/1000, emptying, after crossing the Cameroon coastal plain in its lower reaches, into the Gulf of Guinea, Atlantic Ocean. Rapids break the flow of the NR at the localities of Mbalmayo and Déhané towards the lower reaches (with a slope gradient of 6.7/1000 over 70 km of length). The annual rainfalls are between 1500 and 2000 mm, for a mean annual temperature of about 25 °C, with amplitude of 2.4 °C. This climate exhibits two dry seasons and two rainy seasons (Olivry 1986). In the coastal zone, concerning the 80–100 km of the downstream course of the NR, the climate is very warm and humid (Cameroonian-type), with only one dry season (December–February). The annual mean rainfall is 2000–3500 mm, the annual mean temperature is 26 °C with a 2.8 °C amplitude.

The NR has many small tributaries, such as the So’o River (the relative most important left hand tributary) and the Mfoumou and Afamba rivers to the right (Fig. 1b). The basement rocks of the NR drainage basin (Fig. 1a) belong both to the Pan-African belt (e.g., Yaoundé Group) and the Ntem complex. The Pan-African belt in central Africa (e.g., in Cameroon) consists of Neoproterozoic supracrustal assemblage, variously deformed granitoids, and medium- to high-grade metamorphic rocks. The evolution of this belt is still enigmatic, leading to the formulation of various and divergent tectonic models (Toteu et al. 2004). The Pan-African rocks are interpreted to have formed in a continental collision zone

Fig. 1 **a** Geological map of the South Cameroon (from Toteu et al. 2001) with the outline of the study area and the location of the areas from where the geochemical data of parental rocks were compiled in this study to identify probable source rocks. **b** Simplified map of Nyong River watershed (modified from Olivry 1986) showing the landforms and sample sites



between the West African and Congo craton (Toteu et al. 2001; Kröner and Stern 2004; Toteu et al. 2004). However, some rocks of the studied area, belonging to the Yaoundé Group, such as the low- to high-grade garnet-kyanite metasedimentary gneisses, were interpreted as metamorphosed Neoproterozoic epicontinental deposits linked either to an intracontinental distensive environment or to a passive margin (Nzenti et al. 1988). The Pan-African rocks, encountered toward the upper reaches of the NR, are not only composed mainly of metashales, metagreywackes, quartzites, amphibolites, talcschists, garnetiferous micaschists and gneisses, migmatites, migmatitic gneisses, and granites but also of scarce pre- to syntectonic metaplutonic rocks, including mostly mafic to intermediate rocks (pyriclasites), serpentized chromitic and nickeliferous ultramafic rocks associated with metagabbros, metadiorites, and mafic dykes (Nédelec et al. 1986; Nzenti et al. 1988). These rocks, representing a huge allochthonous nappe unit thrust southward onto the Congo craton (Fig. 1a), were derived from protoliths consisting of a mixture of juvenile Neoproterozoic and Paleoproterozoic sources, as indicated by Sm-Nd isotopic data, without a major contribution of the Archean Congo craton (Penaye et al. 1993; Toteu et al. 1991, 2001).

The NC, consisting of the Nyong and Ntem units, has been mapped in the eastern part of the studied drainage basin. In the middle reaches of the NR, some tributaries, such as the So'o River, flow through the Ntem unit, which consists of remnants of green stone belts (i.e., xenoliths of metasediments and garnet amphibolites) preserved in younger intrusive complexes, charnockites, and other granitoids (Vicat et al. 1996). Towards the Atlantic coast, the studied river drainage basin basement belongs to the Nyong unit, which is made up of reworked felsic and mafic Archean rocks, Tonalitic, Trondhjemitic, and Granodioritic (TTG) suites, metagabbros, anorthosites, charnockites, gneisses, migmatites, amphibolites, alkali metasyenites, garnetites, eclogites, serpentized peridotites, quartzites, and Banded Iron Formations (BIF) (Feybesse et al. 1998; Penaye et al. 2004). Vicat and Pouclet (1995), Vicat et al. (1996), and Pouclet et al. (2007) argued that the Ntem unit experienced pre-Eburnean rifting (older than 2500 Ma) followed by the opening of the Nyong intracratonic basin (2515–2535 Ma), as well as the Eburnean and Pan-African events (Feybesse et al. 1998).

Materials and methods

A total of 20 surface sediment samples (fine and coarse sands) at different intervals, for a distance of about 690 km from near Abong-Mbang locality to the coastal zone north Kribi, were collected from the active flood-plain or the bed-load along the NR (Fig. 2). Due to the accessibility to the river bed and the relief, the drainage basin has been divided into two sectors:

upstream sector (Ups) and downstream sector (Dws). Approximately 3 kg of the alluvium were collected at each sampling site. To ensure that the sediments samples corresponded to recent deposits, they were retrieved at the upper part of the alluviums. The samples and their locations are listed in Table 1. These samples were analyzed for texture (on all samples) and mineralogy (on selected samples). The samples were oven-dried (70 °C) for about 48 h and then homogenized. Sand size particles were separated by wet sieving and size fractions above 0.050 mm by dry sieving using a Ro-Tap Sieve Shaker (for 20 min) at the Faculty of Agronomy and Agricultural Sciences (FASA), Dschang, Cameroon (Folk 1980).

Heavy minerals (~ 150 µm; density > 2.9 g/cm³) were separated using bromoform, as heavy liquid, and identified under a binocular microscope at the Geoscience laboratories, University of Yaoundé I, Cameroon. Seven sediment samples (4 from Ups and 3 from Dws) were selected for mineralogy study, using X-ray diffraction (XRD) method. The XRD results of the studied samples were obtained by using a BRUKER D8 Eco diffractometer provided with a monochromator using a Cu-K α radiation (λ = 1.5406 Å) at 40 kV and 45 mA, at the geology and sedimentary environment laboratories (AGEs), University of Liège, Belgium. The mineralogical identification was done with the software DIFFRAC plus TOPAS. The results obtained are similar to those recorded with classical methods (Carrol 1970; Krumm 1996).

All the 20 sediment samples (10 from Ups and 10 from Dws) for major, trace, including REE, analysis were finely ground in an agate mortar until the material could be sieved through a 0.075-mm sieve. Major element concentrations were determined by X-ray fluorescence spectrometry (XRF) at AGEs. The LOI (loss on ignition) was determined by weighing the samples before and after 2 h of calcination at 1000 °C, using an ARL PERFORM-X 4200. The geochemical standard AWI-1 was used to determine data quality. Analytical precision for major elements was better than \pm 5%, except for SiO₂, Fe₂O₃, and TiO₂ which were occasionally \pm 2%. The trace and REE were analyzed by means of inductively coupled plasma-mass spectrometry (ICP-MS) technique (see Jarvis 1990) at AGEs. Sediment powders were digested by acid attack, using a mixture of LiBO₂ and HNO₃ in a ThermoFisher Scientific Xseries2CCT^{ED} ICP-MS instrument. Samples were prepared as 0.25 g sample mixed with 1.25 g LiBO₂ flux, placed in a carbon crucible and fused in a muffle furnace for 30 min at 1000 °C. The melt was poured into 150 ml of 3.5% HNO₃. The fused and re-dissolved solution was diluted 20 times with 2% double-sub-boiled HNO₃ to obtain the working solution. The analytical accuracy errors, determined by replicates, are generally better than \pm 2%, except for Sc, V, Cr, Co, Ni, Cu, Zn, and Ga, which were at times \pm 5%. The accuracy and precision of the analytical

Table 1 Sampling locations of the Nyong River sediments, with corresponding sample ID and their physical feature (color and texture)

Localities	Sample Id	Latitude (N)	Longitude (E)	Altitude (m)	Color	Texture
Abong-Mbang	Ab1	3° 53' 03.55"	13° 24' 32.66"	950	Reddish brown	Coarse sand
	Ab2	4° 09' 07.18"	13° 03' 28.87"	950	Reddish brown	Coarse sand
Ayos	Ay1	4° 10' 49.83"	12° 45' 37.12"	933	Pale brown	Coarse sand
	Ay2	4° 06' 03.37"	12° 43' 32.33"	922	White	Fine sand
	Ay3	3° 57' 03.08"	12° 36' 54.05"	922	White	Fine sand
	Ay4	3° 48' 46.14"	12° 26' 51.93"	922	White	Fine sand
Akonolinga	Ak1	3° 50' 38.67"	12° 20' 22.71"	862	White	Fine sand
	Ak2	3° 45' 33.58"	12° 10' 18.73"	816	Light brown	Fine sand
	Ak3	3° 37' 58.35"	11° 40' 39.73"	800	Light brown	Fine sand
	Ak4	3° 32' 41.88"	11° 38' 20.81"	784	Light brown	Fine sand
Mbamayo	Mb1	3° 38' 44.91"	11° 33' 00.77"	655	Light brown	Fine sand
	Mb2	3° 32' 06.88"	11° 30' 26.67"	620	Grayish brown	Coarse sand
	Mb3	3° 27' 09.53"	11° 26' 22.82"	598	Brown	Coarse sand
	Mb4	3° 19' 09.80"	11° 22' 36.62"	576	Brown	Fine sand
Makak	Ma1	3° 35' 29.78"	11° 08' 5.69"	420	Brown	Coarse sand
	Ma2	3° 30' 41.66"	10° 57' 34.73"	396	Brown	Coarse sand
Eseka	Es1	3° 33' 35.07"	10° 45' 16.63"	256	Brown	Coarse sand
	Es2	3° 30' 44.05"	10° 36' 51.97"	200	Brown	Coarse sand
Dehane	Dh1	3° 31' 31.17"	10° 18' 54.09"	55	Pale brown	Coarse sand
	Dh2	3° 27' 26.65"	10° 16' 32.84"	25	Pale brown	Coarse sand

methods were recognized using international standard (BHVO-1, SGR-1, JB-3, and GA).

Results

Granulometric and mineralogical characterization

The granulometric analysis results of stream sediments from the NR watershed and their parameters calculated using Folk (1980) formula are shown in Table 2. They display little variation between the Ups and Dws. Samples from the Ups are composed, on average, of 42.11% of fine- to medium-grained particles (Fsd/Msd), 46.86% of coarse to very coarse-grained sand (Csd/Vcsd), 6.5% of clay/silts, and 4.53% of gravels. The mean grain size (Mz) varies from 0.56 to 1.43 in the phi scale (Φ) and the average skewness (Ski) is negative, indicating an excess of coarse materials in the studied sediments (Table 2). They are classified mostly as medium and coarse sands (Folk 1980). The Trask's Sorting Coefficient (So) varies from 1.41 to 2.82 mm and the standard deviation (σ ; graphical method) in the phi scale ($s\Phi$) varies from 0.7 to 0.97, so the sediments are classified as moderately sorted, indicating proximity with source areas. The graphic kurtosis (K_G) average value is 0.7 (platykurtic curves).

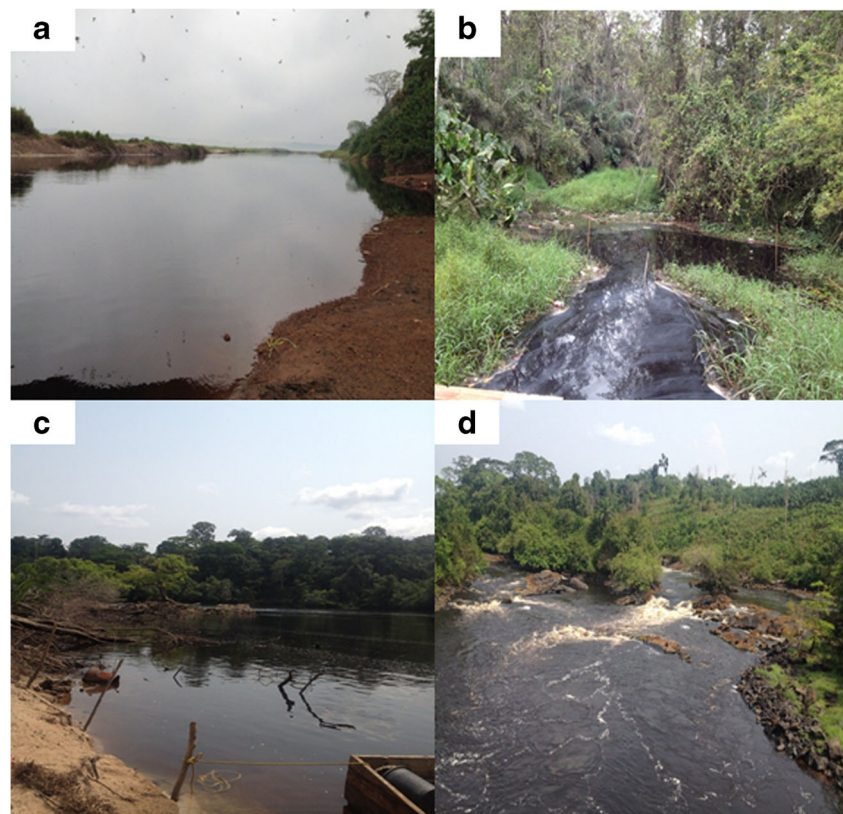
In the Dws, the samples are composed, on average, of 33.86% of fine- to medium-grained particles (Fsd/Msd),

62.58% of coarse- to very coarse-grained sand (Csd/Vcsd), 1.16% of clays/silts, and 2.41% of gravels (Table 2). Mz varies from Φ -0.43 to Φ 0.86 (coarse sand; Folk 1980), indicating sediments are coarser than that in Ups. This is probably due to the contribution, towards the lower reaches, of coarser materials from different tributaries, such as the So'o, Mfoumou, and Afamba rivers. The coarse texture can also be attributed to the little impact of fluvial transport processes in abrading coarser debris, originated from the upper reaches, to smaller sizes and the removal of fine size particles, taken away toward the Atlantic sea, into suspension. The average Ski is positive. The σ (0.58 to 1.35) of Dws sediments indicates moderately well sorted to poorly sorted. The K_G values (> 1) indicate a leptokurtic distribution of sediment particles.

The distribution of heavy minerals is shown in Table 3. Major heavy minerals found in the Ups sediments are opaque minerals (40–70%), kyanites (10–31%), rutiles (7–10%), chloritoids (2–5%), in order of decreasing abundance, while in Dws, they are opaque minerals (31–53%), kyanites (17–40%), zircons (1–10%), diopsides (3–8%), and tourmalines (2–7%).

Table 4 presents the XRD results of the stream sediments studied. Quartz is the most represented mineral, both in Ups and Dws, among kaolinites, feldspars, and hematites. Illites and rutiles are observed only in the Ups (Fig. 3).

Fig. 2 Physical characteristics of Nyong River and of some sampling points: **a** Location of sample Ak1 in an inactive sand bank; **b** river margin near the location of sample Ab1, where the water depth was low; **c** river margin where the sample Ma1 was taken; and **d** Lobe River margin, not far from where Es1 was taken



Major element geochemistry

Major element concentrations are given in Table 5. In the Ups, all the samples show higher concentrations of SiO₂ (mean = 81.07 wt.%). Large variations are observed in the

Al₂O₃ and Fe₂O₃ contents (1.04–12 wt.%, 0.22–21.56 wt.%, respectively). Small variations are observed in TiO₂, MnO, CaO, K₂O, and Na₂O contents. Compared with the Upper Continental Crust (UCC), the sediment are higher in SiO₂, TiO₂, Al₂O₃, Fe₂O₃, and P₂O₅ (Fig.

Table 2 Grain size distribution (wt.%) and textural parameters (Folk 1980) of the Nyong River sediments

Sector	Upstream (<i>n</i> = 10)					Downstream (<i>n</i> = 10)						
	Av AB (<i>n</i> = 2)	Av Ay (<i>n</i> = 4)	Av Ak (<i>n</i> = 4)	Av	± 1σ	Mb1 (<i>n</i> = 1)	Mb-Ma (<i>n</i> = 3)	Av Ma (<i>n</i> = 2)	Av Es (<i>n</i> = 2)	Av Dh (<i>n</i> = 2)	Av	± 1σ
Gravel %	8.24	3.34	2	4.53	3.28	4.2	2.2	1.14	3.1	1.4	2.41	1.26
Csd/Vcsd %	74.3	38.48	27.81	46.86	24.35	40.48	70.19	80.1	61.01	61.11	62.58	14.64
Fsd/Msd %	12.16	50.58	63.6	42.11	26.74	50.28	27.33	18.5	35.79	37.38	33.86	11.88
Silt/clay %	5.3	7.6	6.59	6.5	1.15	5.04	0.28	0.26	0.1	0.11	1.16	2.17
Sorting (So)	2.82	1.42	1.41	1.88	0.81	1.41	1.42	1.41	1.42	1.18	1.37	0.11
Skewness (Ski)	− 0.38	0.16	− 0.12	− 0.11	0.27	− 0.42	0.51	0.18	0.14	0.42	0.17	0.36
Mz (Φ)	0.56	1.33	1.43	1.11	0.48	1.13	0.68	0.36	0.86	− 0.43	0.52	0.6
σ (sΦ)	0.7	0.97	0.8	0.82	0.14	0.63	0.73	0.58	0.68	1.35	0.79	0.32
Kurtosis (K _G)	0.3	1.04	0.76	0.7	0.37	0.97	1	1.43	0.82	4.32	1.71	1.48
Texture	Csd	Fsd	Fsd	–	–	Fsd	Csd	Csd	Csd	Csd	–	–

Mz (Φ): mean grain size in phi scale; σ (sΦ): standard deviation in phi scale; Av: average; AB: Abong-Mbang (Av sample Ab1 and Ab2); Ay: Ayos (Av Ay1, Ay2, Ay3, and Ay4); Ak: Akonolinga (Av Ak1, Ak2, Ak3, and Ak4); Mb1: Mbalmayo; Mb-Ma: Mbalmayo-Makak (Av Mb2, Mb3, and Mb4); Ma: Makak (Av. Ma1 and Ma2); Es: Eseka (Av Es1 and Es2); Dh: Déhane (Av Dh1 and Dh2). Csd: coarse sand; Vcsd: very coarse sand; Fsd: fine sand; Msd: medium sand; clays: $\phi < 2 \mu\text{m}$; Silts: $2 \mu\text{m} < \phi < 50 \mu\text{m}$; Sand: $50 \mu\text{m} < \phi < 200 \mu\text{m}$; gravel $\phi > 200 \mu\text{m}$. From Folk (1980). *n* = total number of samples

Table 3 Heavy mineral distribution (%) in the sediments from Nyong River

Sector	Upstream sector (<i>n</i> = 4)				Downstream sector (<i>n</i> = 4)			
	Ref. code	Ab1	Ay1	Ak2	Ak4	Mb2	Ma1	Es2
Zircon	1	1	2	1	10	1	6	1
Rutile	10	7	9	8	–	–	2	–
Kyanite	10	31	30	20	17	20	40	30
Tourmaline	–	4	1	4	2	5	3	7
Sillimanite	3	1	2	3	4	2	1	1
Chloritoïd	2	4	5	5	3	1	–	–
Garnet	1	3	4	2	7	5	7	11
Hypersthene	–	2	–	1	4	1	1	–
Anatase	–	2	1	–	4	2	2	3
Zoisite	1	1	1	2	–	1	2	2
Augite	–	1	3	1	1	–	1	–
Diopside	2	1	2	3	8	3	4	6
Opaque minerals	70	42	40	50	40	53	31	39
Total	100	100	100	100	100	100	100	100
ZTR index	36.66	20.68	20	26	20	21.05	15.94	13.11

ZTR (zircon-tourmaline-rutile) index = (Z + T + R)*100/total of non-opaque minerals

4a). The enrichment of Fe₂O₃ suggests the derivation of sediments from Fe-rich source rocks. The depletion in K₂O and Na₂O contents may be linked to the low feldspar contents (e.g., Kassi et al. 2015; Armstrong-Altrin et al. 2020). The correlation between SiO₂ versus Na₂O and K₂O (*r* = 0.17 and – 0.52, respectively) are statistically not significant (Table 6), indicating their high Na and K mobility during weathering and neoformation of clay minerals (e.g., Xie and Chi 2016).

In the Dws, the average SiO₂ content (88.75 wt.%) is slightly higher than that of Ups. All the SiO₂ and TiO₂ contents, and most of Al₂O₃, Fe₂O₃, and MnO contents are higher than the UCC (Fig. 4b). All the samples are depleted in CaO, Na₂O, K₂O, and P₂O₅, compared to the UCC. The correlations of SiO₂ versus Al₂O₃ and Fe₂O₃ are significant (*r* =

0.72 and – 0.93, respectively), while they are not significant with the rest of the elements (Table 6).

On the log (Fe₂O₃/Al₂O₃) versus log (Fe₂O₃/K₂O) binary plot (Herron 1988), the Ups samples are classified as Fe–shale, Fe–sand, and quartz arenite, while the in the Dws, samples fall mostly in the fields of Fe–sand (Fig. 5).

Trace element geochemistry

Trace element compositions of NR sediments and their mean concentrations and standard deviation values, per sector, are listed in Table 7. Figure 4c, d shows the UCC-normalized trace element patterns of these sediments (Taylor and McLennan 1985). Among high field strength elements (HFSE; i.e., Zr, Hf, Ta, and Y), in Ups, Zr, Hf, and Ta (343.9 ± 315.6 ppm, 7.62 ± 6.3 ppm, and 1.56 ± 0.92 ppm respectively) are higher than UCC (190 ppm, 5.8 ppm, and 1 ppm, respectively), while Y is lower than the UCC. Zr and Hf show significantly positive correlation (*r* = 1; Table 6). This correlation indicates that Hf is controlled by zircon. The correlation between Zr and Th is not statistically significant (*r* = 0.39), while it is significant for Th versus Al₂O₃ (*r* = 0.74; Table 6), suggesting that the distribution of the Th is monitored by phyllosilicates (Armstrong-Altrin et al. 2015, 2019). The large ion lithophile elements (LILE) such as Ba (23–318 ppm), Rb (2–41 ppm), and Sr (3.4–67 ppm) show wider variations, but their average contents (96.5 ± 101.1, 10.34 ± 12.96, 16.36 ± 19.83, respectively) are lower than the UCC (550, 112, 350, respectively). Strong correlations are observed between Ba and Sr versus Al₂O₃ (*r* = 0.82 and *r* = 0.73, respectively), suggesting that they are mainly hosted by clay minerals.

Table 4 Mineralogical composition (semi-quantitative) of sediments from the Nyong River

Sector	Upstream (<i>n</i> = 4)				Downstream (<i>n</i> = 3)		
	Ref. code	Ab1	Ay3	Ak2	Ak4	Ma2	Es1
Quartz	++++	++++	++++	++++	++++	++++	++++
Kaolinite	–	++	–	–	–	–	–
Illite	–	++	–	–	–	–	–
Feldspars	–	+	–	–	–	+	+
Hematite	+	+	+	+	+	+	+
Rutile	+	+					

++++ very abundant, ++ represented, + poorly represented, – traces

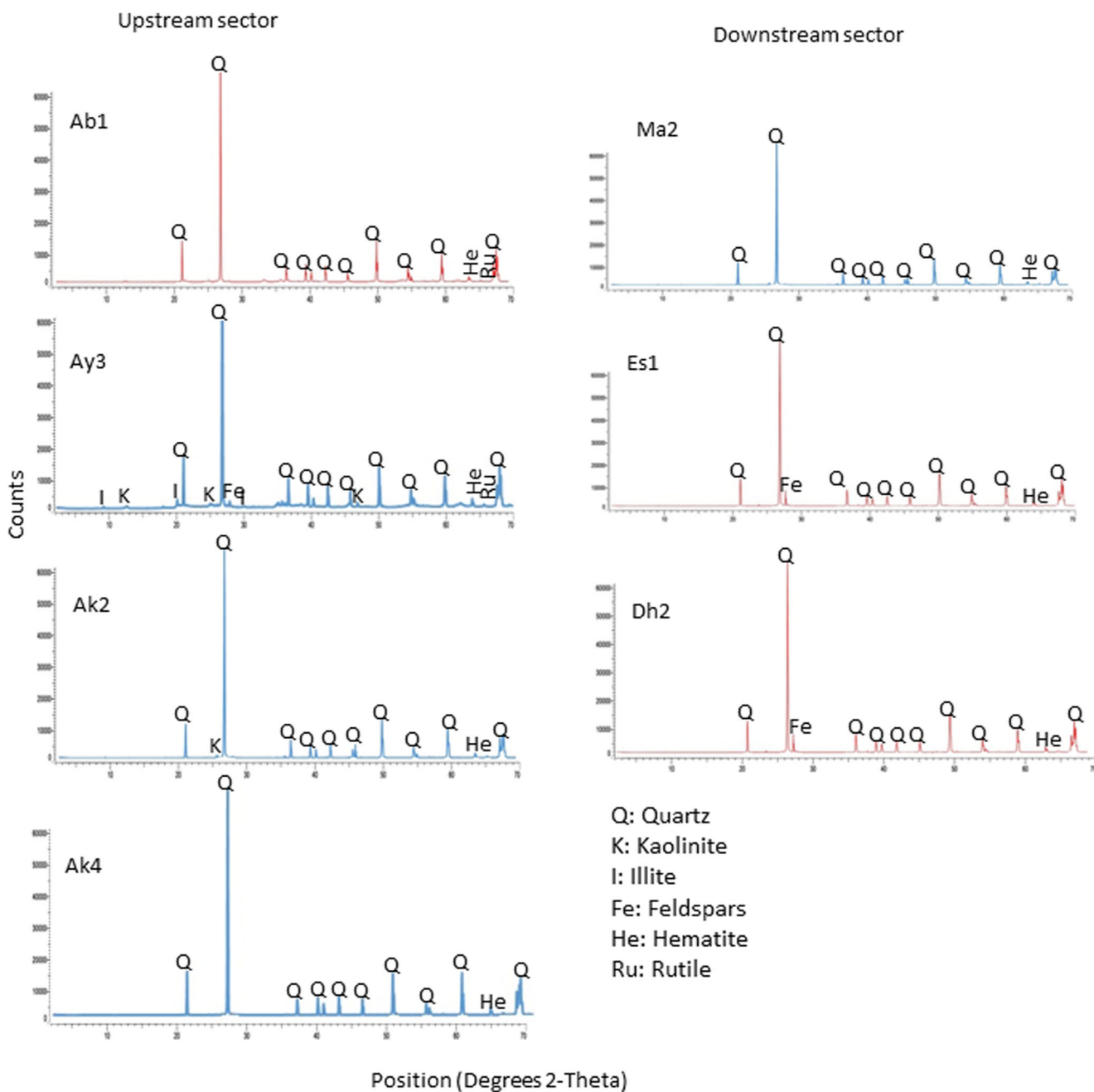


Fig. 3 X-ray diffraction spectra of the Nyong River sediments

The concentrations of transitional trace elements (TTE), such as Co (2.38 ± 1.99 ppm) and Ni (11.37 ± 13.38 ppm), are lower than the UCC, while others like Sc (16.51 ± 7.3 ppm), V (108.5 ± 115.2 ppm), and Cr (124.3 ± 134.4 ppm) are greater than the UCC. TTE such as Co, Cr, Sc, and V, show noticeable correlation with Al_2O_3 (Table 6), indicating that these elements are partially associated with phyllosilicates (Armstrong-Altrin et al. 2015).

In Dws, HFSE such as Zr and Hf are higher than in Ups and also than UCC, and they are not correlated with Al_2O_3 . LILE are also not correlated with Al_2O_3 and are enriched relative to

Ups and depleted, compared to the UCC. V (34 ± 23.36 ppm), Cr (41.09 ± 17.79 ppm), and Ni (4.98 ± 2.18 ppm) are depleted relative to UCC and Ups. The depletion of these TTE is likely related to the supply of felsic detritus.

Rare earth element geochemistry

In the Ups, the Σ REE concentrations vary widely (10.08–281.5 ppm) and are depleted than those of the UCC (146.37 ppm), except in sample Ab2 (Table 8). The UCC-normalized REE patterns (Fig. 6a) are similar for

Table 5 Major element concentrations (wt.%) and element ratios of the Nyong River sediments and average composition of UCC

Location	Upstream sector (n = 10)											±1 σ	
	Ab1	Ab2	Ay1	Ay2	Ay3	Ay4	Ak1	Ak2	Ak3	Ak4	Av		
Ref code													
SiO ₂ (adj)	83.08	67	96.77	79.46	97.66	74.27	66.21	96.61	89.49	97.61	84.82		12.64
SiO ₂	76.92	65.94	96.71	67.35	97.64	71.6	63.06	89.38	86.42	95.72	81.07		13.66
TiO ₂	0.26	2.14	0.38	2.18	0.8	1.25	1.45	0.75	1.24	0.77	1.12		0.66
Al ₂ O ₃	4.79	9	1.9	10.52	1.1	12	8.23	1.9	7.08	1.04	5.76		4.15
Fe ₂ O ₃ [†]	10.21	20.4	0.68	3.44	0.22	9.33	21.56	0.3	1.3	0.37	6.78		8.34
MnO	0.02	0.08	0.01	0.02	0	0.03	0.02	0.01	0.02	0.01	0.02		0.02
MgO	0	0.2	0	0.23	0	0.42	0.24	0	0.03	0	0.11		0.14
CaO	0.11	0.3	0.07	0.12	0.07	0.18	0.09	0.07	0.09	0.05	0.12		0.07
Na ₂ O	0.17	0.12	0.11	0.24	0.12	0.58	0.15	0.11	0.14	1	0.27		0.29
K ₂ O	0.03	0.03	0.08	0.56	0.03	0.94	0.31	0	0.24	0	0.22		0.31
P ₂ O ₅	0.08	0.21	0	0.1	0	0.08	0.13	0	0.01	0	0.06		0.07
LOI	2.93	1	0.73	16.04	0.55	5.08	5.78	4	1.02	0.91	3.8		4.72
Total	95.52	99.42	100.8	100.8	100.5	101.5	101	96.52	97.58	98.96	99.26		2.07
SiO ₂ /Al ₂ O ₃	16.06	7.33	50.9	6.4	88.76	5.97	7.66	47.04	12.21	92.04	14.09		34.27
K ₂ O/Na ₂ O	0.18	0.25	0.73	2.33	0.25	1.62	2.07	0	1.71	0	0.81		0.92
K ₂ O/Al ₂ O ₃	0.01	0	0.04	0.05	0.03	0.08	0.04	0	0.03	0	0.04		0.03
Na ₂ O/Al ₂ O ₃	0.04	0.01	0.06	0.02	0.11	0.05	0.02	0.06	0.02	0.96	0.05		0.29
Fe ₂ O ₃ /K ₂ O	340.3	680	8.5	6.1	7.3	9.9	69.5	-	5.4	-	112		225
CIA (%)	93.7	95.5	82.8	91.5	75.5	85.1	95	86	91.8	80.3	87.72		6.82
PIA (%)	94.3	97.4	85.5	96.4	76.7	91	98.8	86	94.9	80.3	90.13		7.63
CIW	89.54	97.4	83.99	96.57	77.2	91.67	98.8	86.04	95.03	80.28	89.65		7.55
ICV	1.54	1.9	0.69	0.64	1.38	0.91	2.06	0.77	0.44	1.43	1.18		0.56
Location	Downstream sector (n = 10)												
Ref code	Mb1	Mb2	Mb3	Mb4	Ma1	Ma2	Es1	Es2	Dh1	Dh2	Av	+1 σ	UCC
SiO ₂ (adj)	89.76	86.59	97.22	92.26	87.53	92.9	93.4	94.32	94.21	91.88	92.01	3.24	-
SiO ₂	89.12	79.19	94.93	86.69	84.99	87.24	91.33	93.48	91.3	89.13	88.74	4.55	66
TiO ₂	0.77	0.28	0.12	0.84	3.31	1.42	0.24	0.15	0.38	1.24	0.88	0.97	0.5
Al ₂ O ₃	4.4	5.06	2.28	4.56	4.43	2.12	3.45	2.65	3.34	3.97	3.63	1.02	15.2
Fe ₂ O ₃ [†]	1.84	6.4	0.41	1.57	3.6	2.9	1.56	1.38	1.2	1.62	2.25	1.71	4.5
MnO	0.04	0.01	0.01	0.01	0.05	0.02	0.03	0.03	0.03	0.03	0.03	0.01	0.1
MgO	0.09	0	0	0	0.07	0.01	0.03	0.03	0.1	0.14	0.05	0.05	2.2
CaO	0.35	0.1	0.09	0.07	0.17	0.08	0.25	0.26	0.27	0.33	0.2	0.11	4.2
Na ₂ O	0.66	0.15	0.12	0.1	0.24	0.09	0.44	0.5	0.28	0.28	0.29	0.19	3.9
K ₂ O	1	0.24	0.04	0.12	0.24	0.03	0.25	0.33	0.27	0.26	0.28	0.27	3.4
P ₂ O ₅	0.01	0.02	0.01	0	0	0	0.02	0.01	0	0.01	0.01	0.01	0.17
LOI	0.83	1.31	0.99	0.76	1.9	1.42	1.08	1.43	0.83	0.76	1.13	0.38	
Total	100.1	95.76	99	97.16	99.01	95.32	98.67	100.5	101	97.77	98.43	1.92	
SiO ₂ /Al ₂ O ₃	20.25	15.65	41.64	19.01	19.19	41.15	26.47	35.28	27.34	22.45	24.47	4.44	
K ₂ O/Na ₂ O	1.52	1.6	0.33	1.2	1	0.33	0.57	0.66	0.96	0.93	0.91	0.45	
K ₂ O/Al ₂ O ₃	0.23	0.05	0.02	0.05	0.05	0.01	0.07	0.09	0.08	0.06	0.07	0.06	
Na ₂ O/Al ₂ O ₃	0.15	0.03	0.05	0.02	0.05	0.04	0.13	0.19	0.08	0.07	0.08	0.19	
Fe ₂ O ₃ /K ₂ O	1.84	26.67	10.25	13.08	15	96.67	6.24	4.18	4.44	6.23	18.46	28.41	
CIA (%)	61.3	88.8	85.7	91.5	82.1	86.7	78.1	61.4	72	75.1	78.27	10.79	
PIA (%)	66.1	92.7	86.9	93.8	85.6	87.7	82	63.7	75.4	78.1	81.2	10.36	
CIW	72.15	93	87.11	93.98	86.28	87.83	83.14	66.95	77.2	79.23	82.69	8.78	
ICV	1.19	0.38	0.37	0.55	1.74	1.9	0.83	1.34	0.88	1.09	1.03	0.53	

LOI: Loss of ignition

CIA (%) = [Al₂O₃ / (Al₂O₃ + CaO* + Na₂O + K₂O)] × 100 from Nesbitt and Young (1982)

PIA (%) = [Al₂O₃ - K₂O / (Al₂O₃ + CaO* + Na₂O - K₂O)] × 100 from Nesbitt and Young (1982) and Fedo et al. (1995)

CIW = (Al₂O₃ / (Al₂O₃ + CaO* + Na₂O)) × 100 from Harnois (1988)

ICV = (FeO₃ + K₂O + Na₂O + CaO + MgO + Mn + TiO₂) / Al₂O₃ from Cox et al. (1995)

The UCC values are cited from Taylor and McLennan (1985) and McLennan (2001)

(SiO₂)_{adj.} refers to SiO₂ contents recalculated to an anhydrous basis and adjusted to 100%

Av. = average. 1σ = one standard deviation. Fe₂O₃[†] = Total Fe expressed as Fe₂O₃. n = total number of samples

Table 6 Correlation matrix of geochemical data from the Nyong River sediments. Pearson's correlation coefficients calculated using the XLSTAT software (level of statistical significance: $p < 0.05$)

	SiO ₂	TiO ₂	Al ₂ O ₃	Fe ₂ O ₃	MnO	MgO	CaO	Na ₂ O	K ₂ O	P ₂ O ₅	Ba	Ni	Cr	Sc	Co	Ga	Hf	Nb	Rb	Sr	Ta	Th	U	V	Zr	Y	ΣREE										
SiO ₂	1																																				
TiO ₂	-0.71	1																																			
Al ₂ O ₃	-0.87	0.74	1																																		
Fe ₂ O ₃	-0.82	0.47	0.58	1																																	
MnO	-0.64	0.64	0.58	0.7	1																																
MgO	-0.78	0.65	0.89	0.57	0.47	1																															
CaO	-0.65	0.64	0.65	0.66	0.96	0.58	1																														
Na ₂ O	0.17	-0.08	-0.05	-0.19	-0.12	0.14	-0.14	1																													
K ₂ O	-0.52	0.42	0.8	0.16	0.09	0.87	0.24	0.21	0.23	0.23	1																										
P ₂ O ₅	-0.9	0.71	0.71	0.90	0.85	0.64	0.84	-0.22	0.84	0.95	0.39	1																									
Ba	-0.59	0.54	0.82	0.23	0.24	0.91	0.4	0.19	0.95	0.17	0.63	0.25	1																								
Ni	-0.61	0.1	0.46	0.54	0.48	0.31	0.54	-0.11	0.17	0.63	0.14	0.68	0.1	1																							
Cr	-0.80	0.44	0.54	0.97	0.76	0.45	0.72	-0.25	0.04	0.92	0.14	0.52	0.92	0.72	1																						
Sc	-0.88	0.7	0.69	0.94	0.82	0.69	0.80	-0.16	0.26	0.98	0.4	0.82	0.82	0.82	0.82	1																					
Co	-0.75	0.73	0.88	0.52	0.75	0.85	0.85	0.06	0.67	0.76	0.8	0.54	0.53	0.53	0.53	0.53	1																				
Ga	-0.93	0.77	0.91	0.8	0.77	0.87	0.82	-0.07	0.59	0.92	0.69	0.57	0.78	0.92	0.91	0.91	0.91	1																			
Hf	-0.5	0.77	0.60	0.09	0.23	0.55	0.34	-0.04	0.53	0.43	0.68	0.16	0.1	0.38	0.64	0.55	0.55	0.55	1																		
Nb	-0.56	0.83	0.64	0.26	0.18	0.66	0.26	-0.05	0.58	0.44	0.66	-0.06	0.17	0.47	0.53	0.59	0.88	0.88	0.88	1																	
Rb	-0.47	0.38	0.75	0.09	0.08	0.84	0.25	0.25	0.99	0.21	0.97	0.21	0.00	0.23	0.69	0.56	0.57	0.55	0.55	0.55	1																
Sr	-0.49	0.31	0.73	0.19	0.13	0.87	0.32	0.26	0.96	0.27	0.96	0.29	0.09	0.29	0.71	0.59	0.47	0.46	0.46	0.46	0.46	1															
Ta	-0.52	0.81	0.59	0.23	0.12	0.61	0.18	-0.02	0.55	0.38	0.61	-0.14	0.13	0.43	0.46	0.53	0.83	0.99	0.99	0.99	0.99	0.99	1														
Th	-0.89	0.75	0.74	0.92	0.83	0.68	0.81	-0.2	0.28	0.98	0.4	0.51	0.91	0.99	0.73	0.93	0.41	0.51	0.23	0.28	0.28	0.28	0.47	1													
U	-0.91	0.71	0.78	0.80	0.45	0.8	0.47	-0.12	0.54	0.8	0.6	0.34	0.71	0.85	0.62	0.86	0.54	0.73	0.48	0.48	0.48	0.71	0.85	1													
V	-0.86	0.51	0.61	0.99	0.62	0.59	0.58	-0.22	0.2	0.88	0.26	0.5	0.94	0.93	0.49	0.8	0.16	0.36	0.13	0.2	0.2	0.34	0.92	0.87	1												
Zr	-0.48	0.76	0.58	0.07	0.21	0.53	0.32	-0.05	0.52	0.41	0.67	0.15	0.08	0.36	0.62	0.53	0.1	0.88	0.56	0.46	0.84	0.39	0.53	0.15	1												
Y	-0.73	0.82	0.85	0.35	0.51	0.81	0.61	0.03	0.71	0.65	0.85	0.38	0.35	0.61	0.9	0.82	0.9	0.79	0.74	0.69	0.72	0.63	0.68	0.39	0.88	1											
ΣREE	-0.6	0.71	0.54	0.64	0.97	0.43	0.95	-0.2	0.04	0.85	0.23	0.44	0.72	0.8	0.74	0.75	0.38	0.31	0.04	0.08	0.25	0.82	0.45	0.58	0.37	0.57	1										
Downstream sector (n = 10)																																					
SiO ₂	1																																				
TiO ₂	-0.38	1																																			
Al ₂ O ₃	-0.72	0.25	1																																		
Fe ₂ O ₃	-0.93	0.27	0.55	1																																	
MnO	0.09	0.59	0.15	-0.08	1																																
MgO	0.14	0.29	0.21	-0.23	0.67	1																															
CaO	0.35	-0.07	0.11	-0.33	0.67	0.83	1																														
Na ₂ O	0.34	-0.18	0.09	-0.26	0.62	0.44	0.84	1																													
K ₂ O	0.02	-0.04	0.33	-0.06	0.45	0.39	0.61	0.78	1																												
P ₂ O ₅	-0.07	-0.53	0.18	0.26	-0.19	-0.16	0.2	0.33	0.14	1																											
Ba	0.12	0	0.27	-0.15	0.56	0.48	0.71	0.84	0.99	0.13	1																										
Ni	-0.04	0.53	0.16	0.15	0.89	0.43	0.54	0.59	0.29	0.15	0.40	1																									
Cr	-0.44	0.63	0.08	0.48	0.36	0.31	0.05	-0.17	-0.19	0.04	-0.14	0.52	1																								
Sc	-0.28	0.94	0.13	0.28	0.71	0.3	0.86	0.84	0.64	0.17	0.74	0.86	0.28	1																							
Co	0.16	0.3	0.21	-0.1	0.91	0.7	0.86	0.84	0.64	0.17	0.74	0.86	0.28	0.43	1																						
Ga	-0.41	0.57	0.43	0.42	0.64	0.33	0.28	0.39	0.69	-0.04	0.68	0.58	0.38	0.58	0.62	1																					
Hf	-0.29	0.95	0.18	0.27	0.69	0.23	-0.04	-0.04	0.02	-0.42	0.08	0.66	0.58	0.98	0.41	0.65	1																				
Nb	-0.27	0.91	0.03	0.27	0.52	0.13	-0.19	-0.21	-0.04	-0.44	-0.01	0.49	0.59	0.92	0.25	0.63	0.95	1																			
Rb	-0.04	-0.06	0.35	0.01	0.38	0.35	0.55	0.71	0.99	0.19	0.96	0.24	-0.17	-0.09	0.59	0.71	0.01	-0.03	1																		
Sr	0.14	0.01	0.25	-0.17	0.59	0.48	0.72	0.86	0.98	0.13	1.0																										

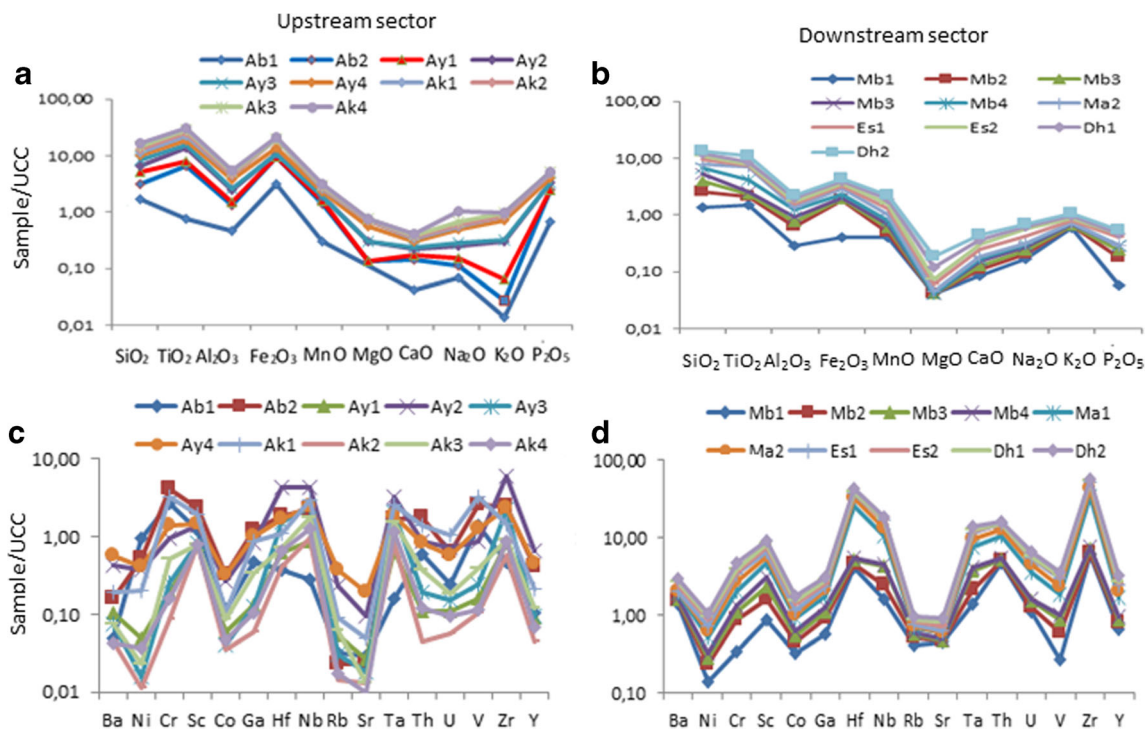


Fig. 4 UCC-normalized major and trace element patterns of the Nyong River sediments. Normalization values are from Taylor and McLennan (1985). **a**, **c** Upstream sector and **b**, **d** downstream sector

all the samples with pronounced positive Ce anomalies and no Eu anomaly. The chondrite-normalized REE patterns (Fig. 6c) are comparable for all the samples with enriched light REE (LREE; La, Ce, Pr, Nd, and Sm) relative to heavy REE (HREE; Gd, Tb, Dy, Ho, Er, Tm, Yb, and Lu). Marked positive Ce and low negative Eu anomalies are observed ($Ce/Ce^* = 1.67 \pm 2.37$ and $Eu/Eu^* = 0.64 \pm$

0.14 , respectively). The $(La/Sm)_{cn}$ and $(Gd/Yb)_{cn}$ (3.93–7.32 and 1.08–2.33, respectively) show marked LREE and low HREE fractionations (where the subscript $_{cn}$ refers to chondrite-normalized values). The REE and Y show some correlation with Al_2O_3 ($r = -0.54$ and $r = 0.85$, respectively), implying that these elements may be hosted in phyllosilicates (Mongelli et al. 2006). The high correlation between REE and TiO_2 in the studied samples ($r = 0.71$; Table 6) suggests the presence of Ti-bearing minerals (i.e., rutile; Ross and Bustin 2009; Fu et al. 2011), as indicated by the DRX results (Fig. 3).

In the Dws, the $\sum REE$ concentrations vary between 16.1 and 441.7 ppm and are depleted than that of the UCC, except in samples Mb1, Ma1, and Ma2 (Table 8). The UCC-normalized REE patterns (Fig. 6b) are similar for all the samples with noticeably negative Eu anomalies and no Ce anomaly. The chondrite-normalized REE patterns (Fig. 6d) are almost comparable for all the samples with enriched LREE relative to HREE. The $(La/Sm)_{nc}$ (4.3–5.77) show marked LREE fractionation. Except sample Mb1, $(Gd/Yb)_{nc}$ vary between 0.86 and 2.68, indicating low HREE fractionation. The REE and Y show no or low correlation with Al_2O_3 ($r = 0.26$ and $r = 0.29$, respectively), implying that these elements may be hosted in accessory phases (Mongelli et al. 2006). The low correlation between REE and TiO_2 ($r = 0.67$) in Dws compared to Ups (r

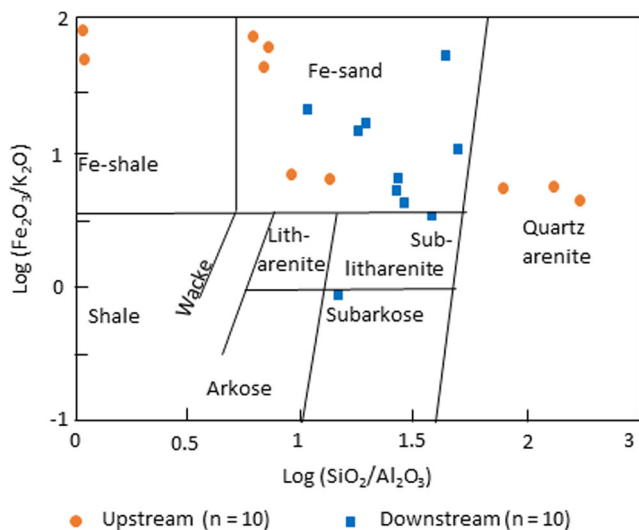


Fig. 5 Geochemical classification of the Nyong River sediments, using a $\log (Fe_2O_3/Al_2O_3)$ versus $\log (Fe_2O_3/K_2O)$ diagram (after Herron 1988)

Table 7 Trace element concentrations (ppm) and element ratios of the Nyong River sediments and average composition of UCC

Location	Upstream sector ($n = 10$)												
	Ref code	Ab1	Ab2	Ay1	Ay2	Ay3	Ay4	Ak1	Ak2	Ak3	Ak4	Av	$\pm 1\sigma$
Ba	27	89	57	237	41	318	107	25	41	23	96.5	101.1	
Ni	41	23	2.2	16.4	0.7	18.3	9	0.5	1	1.6	11.37	13.38	
Cr	245	373	17.7	86	23	126	302	8	47	14.9	124.3	134.4	
Sc	16.1	31	10.5	18.7	11.3	19.5	26	10.5	10.6	10.9	16.51	7.3	
Co	1.9	5.4	1	4.5	0.7	5.6	1.8	0.6	1.5	0.8	2.38	1.99	
Ga	7.9	20	2.2	14.3	2.1	17.2	14.6	1	5.7	1.8	8.68	7.21	
Hf	2.1	10.6	3.6	25	8.7	9.7	6.3	2.4	4.1	3.7	7.62	6.83	
Nb	3.3	27	10.5	51	29	29	36	11.6	21	14.8	23.32	14.09	
Rb	3.6	2.6	6	26	3.5	41	10	1.6	7.1	2	10.34	12.96	
Sr	10.1	8.1	9.5	33	6.4	67	16.9	4.6	4.6	3.4	16.36	19.83	
Ta	0.16	1.67	0.65	3.3	1.98	1.83	2.5	0.83	1.5	1.15	1.56	0.92	
Th	6.2	19.1	1.19	9.2	2.1	8.7	14.5	0.47	3.9	1.26	6.66	6.26	
U	0.69	1.75	0.3	1.98	0.43	1.62	2.9	0.16	0.51	0.26	1.06	0.94	
V	146	267	16.8	93	26	132	340	11.2	41	12	108.5	115.2	
Zr	90	469	154	1147	422	432	281	108	175	161	343.9	315.6	
Y	2.3	9	2	14.2	2.1	10	4.6	0.97	2.6	1.53	4.93	4.53	
Cu	11.6	55	3.1	16.3	1.5	17.6	44	1.9	1.7	4.2	15.69	18.99	
Zn	16.5	59	5.9	34	8	36	34	4.2	14.7	7.5	21.98	18.01	
Ge	0.77	1.39	0.69	1.18	0.7	1.44	1.4	0.66	0.97	0.76	1	0.33	
Cs	0.2	0.2	0.31	1.88	0.18	2	0.51	0.11	0.34	0.2	0.6	0.72	
W	0.34	1.04	0.53	2.5	1.35	1.52	1.64	0.71	0.91	0.42	1.1	0.67	
Pb	10.6	30	2.8	19	2.9	13.5	21	2.3	3.3	3.9	10.93	9.72	
Zr/Hf	42.86	44.25	42.78	45.88	48.51	44.54	44.6	45	42.68	43.51	44.46	1.77	
Cr/Th	39.52	19.53	14.87	9.35	10.95	14.48	20.83	17.02	12.05	11.83	17.04	8.73	
V/Cr	0.6	0.72	0.95	1.08	1.13	1.05	1.13	1.4	0.87	0.81	0.97	0.23	
Th/Sc	0.39	0.62	0.11	0.49	0.19	0.45	0.56	0.04	0.37	0.12	0.33	0.2	
Th/U	8.99	10.91	3.97	4.65	4.88	5.37	5	2.94	7.65	4.85	5.92	2.47	
Rb/Sr	0.36	0.32	0.63	0.79	0.55	0.61	0.59	0.35	1.54	0.59	0.63	0.35	
Ni/Co	21.58	4.26	2.2	3.64	1	3.27	5	0.83	0.67	2	4.45	6.2	
U/Th	0.11	0.09	0.25	0.215	0.21	0.19	0.2	0.34	0.13	0.21	0.19	0.07	
Zr/Sc	5.59	15.13	14.67	61.34	37.35	22.15	10.81	10.29	16.51	14.77	20.86	16.62	
Rb/Sr	0.36	0.32	0.63	0.79	0.55	0.61	0.59	0.35	1.54	0.59	0.63	0.35	
Location	Downstream sector ($n = 10$)												
Ref code	Mb1	Mb2	Mb3	Mb4	Ma1	Ma2	Es1	Es2	Dh1	Dh2	Av	$\pm 1\sigma$	UCC
Ba	765	61	50	41	160	29	167	185	154	173	178.5	215.2	550
Ni	6.2	3.9	2.3	1.8	8.8	4.2	7	6.3	3.8	5.5	4.98	2.18	44
Cr	31	48	25	17.9	63	62	45	27	27	65	41.09	17.79	92.3
Sc	11.6	10.6	10.1	9.9	21	14	11.9	10.9	11.4	12.8	12.42	3.26	13.6
Co	5.5	2.1	1.8	1.2	4.7	2	4.2	3.9	3.2	4.2	3.28	1.44	17
Ga	9.9	5.8	3.2	2.5	8.8	5.2	3.4	3.4	3.5	4.4	5.01	2.50	17
Hf	24	2.1	4	1.83	35	36	9.4	3.4	5.1	16.3	13.71	13.47	5.8
Nb	19.2	9.8	22	3.8	72	36	4.8	3	7.7	15.9	19.42	21.12	12
Rb	46	11.7	6.1	4.6	7.7	3.8	7	7.9	8.1	8.7	11.16	12.44	112
Sr	156	5.9	6.3	5.3	33	5.8	37	39	27	33	34.83	44.89	350
Ta	1.4	0.75	1.61	0.26	3.4	2.2	0.3	0.17	0.55	1.16	1.18	1.02	1
Th	50	4	2.7	1.21	57	24	2.4	2	1.25	4	14.86	21.53	10.7
U	3.1	0.49	0.61	0.28	5.7	2.7	0.6	0.33	0.45	1.68	1.59	1.77	2.8

Table 7 (continued)

Location	Downstream sector ($n = 10$)												UCC
	Mb1	Mb2	Mb3	Mb4	Ma1	Ma2	Es1	Es2	Dh1	Dh2	Av	$\pm 1\sigma$	
V	29	35	30	12.5	89	58	19.5	14	20	33	34	23.36	107
Zr	1118	88	172	74	5145	1677	442	155	242	720	983.3	1553	190
Y	14.5	2.9	2.2	1.49	16	8.3	2.3	1.7	3.3	13.2	6.6	5.87	22
Cu	1.7	2	3.5	2.8	7.8	52	4.7	3	3.3	4.8	8.56	15.36	
Zn	22	14.8	13.6	8.8	32	61	19.3	16.7	19.1	23	23.03	14.73	
Ge	0.93	1.04	0.75	0.76	0.88	0.75	0.71	0.62	0.67	0.72	0.78	0.13	
Cs	0.54	0.61	0.33	0.21	0.25	0.19	0.19	0.18	0.21	0.22	0.29	0.16	
W	0.37	0.75	1	0.14	1.46	1.25	0.2	0.09	0.31	0.68	0.63	0.48	
Pb	13.9	4.5	2.8	2.4	13.7	50	3.3	3.5	3.4	4	10.15	14.66	
Zr/Hf	46.58	41.9	43	40.44	147	46.58	47.02	45.59	47.45	44.17	54.97	32.42	
Cr/Th	0.62	12	9.26	14.79	1.11	2.58	18.75	13.5	21.6	16.25	11.05	7.46	
V/Cr	0.94	0.73	1.2	0.7	1.41	0.94	0.43	0.52	0.74	0.51	0.81	0.31	
Th/Sc	4.31	0.38	0.27	0.12	2.71	1.71	0.2	0.18	0.11	0.31	1.03	1.44	
Th/U	16.13	8.16	4.43	4.32	10	8.89	4	6.06	2.78	2.38	6.71	4.21	
Rb/Sr	0.29	1.98	0.97	0.87	0.23	0.66	0.19	0.2	0.3	0.26	0.6	0.57	
Ni/Co	1.13	1.86	1.28	1.5	1.87	2.1	1.67	1.62	1.19	1.31	1.55	0.33	
U/Th	0.06	0.12	0.23	0.23	0.1	0.11	0.25	0.17	0.36	0.42	0.2	0.12	
Zr/Sc	96.38	8.3	17.03	7.47	245	119.8	37.14	14.22	21.23	56.25	62.28	74.9	
Rb/Sr	0.29	1.98	0.97	0.87	0.23	0.66	0.19	0.2	0.3	0.26	0.6	0.57	

The UCC values are cited from Taylor and McLennan (1985)

Av. = average, 1σ = one standard deviation, n = total number of samples

= 0.71) suggests the relative less abundance of Ti-bearing minerals (Ross and Bustin 2009; Fu et al. 2011).

Discussions

Controls on texture, sediment maturity, and recycling

The texture of the sediments studied (distribution of grain size) did not exhibit a normal regular trend from the upper reaches of NR towards the lower reaches, since the percentage of the coarse and very coarse sands ($-1 - 1\phi$) is slightly higher in the Dws (62.58 ± 14.64 wt%), compared to the Ups (46.86 ± 24.35 wt%). This indicates that the bulk hydraulic energy of the NR does not fully control the grain size of the sediments, suggesting noticeable input of coarser materials from different tributaries.

Hydraulic sorting of the detrital grains can affect the chemical composition of the sediments, leading finally to compositional mature sediments (Gromet et al. 1984; McLennan 1989). Textural maturity of sediments can be depicted using the $\text{SiO}_2/\text{Al}_2\text{O}_3$, $\text{Al}_2\text{O}_3/\text{Na}_2\text{O}$, and $\text{K}_2\text{O}/\text{Na}_2\text{O}$ ratios (Cox et al. 1995; Chen et al. 2014; Khan and Khan 2015;

Madhavaraju 2015) since high values of these ratios (> 6 , > 5 , and > 1 , respectively, illustrate compositionally matured sediments. Basic igneous rock has $\text{SiO}_2/\text{Al}_2\text{O}_3$ ratio of 3, while this ratio is about 5 in the acid igneous rocks, hereafter the values > 5 in clastic sediments indicate sediment maturity and values > 10 indicate high maturity and recycling (Bakkiaraj et al. 2010; Armstrong-Altrin et al. 2013; Wang and Zhou 2013; Hernández-Hinojosa et al. 2018). The $\text{SiO}_2/\text{Al}_2\text{O}_3$ ratios vary from 6.4 to 92.04 with an average of 14.09 ± 3.3 in the Ups and from 15.65 to 41.64 (average = 24.47 ± 4.44) in Dws, indicating a high textural maturity for most samples. $\text{Al}_2\text{O}_3/\text{Na}_2\text{O}$ and $\text{K}_2\text{O}/\text{Na}_2\text{O}$ ratios of NR sediments in Ups and in Dws also suggest high maturity for several sediment samples. On the other hand, mature sediments, resulting in sorting processes, are characterized by the less abundance of alkali feldspar relative to aluminosilicates (Cox et al. 1995). This relationship can be monitored by the $\text{K}_2\text{O}/\text{Al}_2\text{O}_3$ ratio. This ratio > 0.5 suggests a significant quantity of alkali feldspar and < 0.5 suggests the depletion of alkali feldspar relative to aluminosilicates. The $\text{K}_2\text{O}/\text{Al}_2\text{O}_3$ ratios of NR sediments in Ups ($0-0.08$ and 0.04 ± 0.07) and in Dws ($0.01-0.23$ and 0.07 ± 0.06), indicate depletion of alkali

feldspars relative to aluminosilicates during the hydraulic sorting of the detrital grains.

The Index of Chemical Variability (ICV) can also be used to determine the compositional maturity of sediments (Cox et al. 1995). This index, which reflects the non-quartz component of sediments, is formulated as follows: $ICV = (Fe_2O_3 + K_2O + Na_2O + CaO + MgO + Mn + TiO_2)/Al_2O_3$. Generally, typical rock-forming minerals such as k-feldspars, plagioclases, amphiboles, and pyroxenes have ICV value of > 1 , whereas alteration products like kaolinite, illite, and muscovite have ICV value < 1 (Cox et al. 1995; Cullers 2000). In fact, ICV values decrease due to conversion of primary minerals to Al-bearing clays. Hence, variability in ICV values may be due to both variation in source rock composition and difference in weathering processes (Cox et al. 1995). The ICV values of NR sediments range between 0.64 and 2.06 in the Ups. In the Dws, they vary between 0.37 and 1.74. This result suggests that some of the studied sediment samples in both sectors comprise rock forming minerals (i.e., k-feldspars), as revealed by the DRX results (Fig. 3).

The degree of sorting and recycling during the deposition of sediments can be assessed by the contents of Zr and Hf, which are HFSE present in zircon (Armstrong-Altrin 2020). Generally, high contents of these elements are related to recycled effect. The average Zr contents in the Ups (343.9 ± 315.6 ppm) is relatively low, while it is high (983.3 ± 1553.5 ppm) in the Dws. Similarly, the average Hf contents in the Ups (7.62 ± 6.83 ppm) is relatively low, while it is high (13.71 ± 13.47 ppm) in the Dws. This result shows different concentrations of Zr and Hf between Ups and Dws samples, indicating a sorting-related fractionation. This fractionation is accompanied by a less pronounced recycled effect, documented in the ternary Al_2O_3 – TiO_2 –Zr diagram (Garcia et al. 1994; Fig. 7). The recycled effect of the sediments studied, can also be documented by the zircon-tourmaline-rutile (ZTR) index. This index is the percentage of ultrastable minerals over other transparent heavy minerals (Garzanti and Ando 2007). $ZTR < 75\%$ implies immature to submature sediments, whereas $ZTR > 75\%$ indicates mineralogically matured sediments (Hubert 1962). In this study, the ZTR vary between 13.11 and 36.66, signifying recycling and sorting of the sediments.

Source area weathering

During weathering processes, feldspars, as well as other primary minerals, from crystalline bedrocks are progressively transformed into clays, secondary oxides, and hydroxides (Nesbitt and Young 1984; Fedo et al. 1995; Nesbitt et al. 1997), the rate of transformation being related to the degree of weathering, among other factors such as paleoclimate and tectonism. Thus, excluding the effect of other aforementioned factors, the proportion of feldspars in sediments is thought to

reflect paleoweathering intensity. The proportion of feldspars, which are residual minerals in the NR sediments, is very low (Table 4), indicating that the weathering was strong enough to dissolve most of the feldspars or the physical erosion proceeded at a rate which was lesser than the rate of chemical weathering. This could be in accordance with the tectonic stability of the region from the beginning of the Paleozoic time (~ 550 Ma) until now (Vicat and Pouclet 1995; Vicat et al. 1996; Feybesse et al. 1998; Pouclet et al. 2007). The absence of recent tectonic activity favors intense chemical weathering and promotes low erosion rates, which are enhanced by the heavy seasonal rains in the NR watershed and in the entire equatorial coastal region.

Paleoweathering in the source area can also be estimated through various different types of weathering indices such as the Chemical Index of Weathering (CIW; Harnois 1988), the Plagioclase Index of Alteration (PIA; Fedo et al. 1995), and the Chemical Index of Alteration (CIA; Nesbitt and Young 1982). The CIA has been extensively used to characterize weathering processes (e.g., Armstrong-Altrin 2009; Nagarajan et al. 2007; Nguetchoua et al. 2019a, 2019b). The CIA value is calculated using the following equation: $CIA = (Al_2O_3/(Al_2O_3 + Na_2O + CaO^* + K_2O))^*100$, using molecular proportion, as recommended by Nesbitt and Young (1982). In this formula, the CaO^* represents Ca in silicate minerals alone. In this study, CaO contents were corrected for phosphate, using P_2O_5 (apatite) as follows: $CaO^* = CaO - 10(P_2O_5)/3$. Since some of the CaO contents are higher than those of Na_2O contents, the CaO^* has been calculated using the McLennan (1993) proposed method, formulated as follows (after the P_2O_5 correction): (1) if the content of CaO is less or equal to the Na_2O content, then the CaO value is used for further calculation and (2) if the CaO content is higher than Na_2O , then Na_2O value is considered as CaO^* (e.g., Roddaz et al. 2006; Újvári et al. 2008). For the interpretation, it is worth noting that unweathered igneous rocks have CIA values close to 50, while values up to 100 are due to an intense weathering, which produce residual clay enriched in kaolinite, gibbsite, chlorite and Al-oxihydroxides. The calculated CIA values are presented in Table 5. The Ups and Dws samples show almost all CIA values higher ($CIA = 87.72 \pm 6.82$ and 78.27 ± 10.79 , respectively) than that of average sediment (about 65–70; McLennan 1993). The observed higher CIA values indicate the high intensity of chemical weathering in the source areas. The slight difference between the CIA values of Ups and Dws may be due to the different sources of sediments or to a grain size effect, due to sorting. It has been reported that variation in the CIA values in the same river may be due to hydrodynamic sorting (e.g., Shao and Yang 2012). Different source rocks may also explain the differences between the CIA. The sediments from Ups receive contribution mainly from the Yaoundé Group which were affected by the Pan-African orogeny, whereas the sediments from Dws

Table 8 Rare earth element concentrations (ppm) and element ratios of the Nyong River sediments and average composition of UCC and chondrite

Location	Upstream sector (<i>n</i> = 10)											
Ref. code	Ab1	Ab2	Ay1	Ay2	Ay3	Ay4	Ak1	Ak2	Ak3	Ak4	Av	± 1σ
La	9	15.1	3.8	19	6.1	14.6	10.1	3.4	10.8	2.4	9.43	5.59
Ce	24	240	6.6	38	11.4	30	2.1	4.7	22	4.2	38.3	71.92
Pr	1.82	3.2	0.76	4	1.2	3.3	2.1	0.59	2.6	0.48	2	1.25
Nd	6.3	11.5	2.5	14.7	4	11.5	7.2	1.82	9.3	1.64	7	4.6
Sm	1.14	2.4	0.45	2.7	0.65	2.2	1.41	0.29	1.55	0.31	1.31	0.9
Eu	0.2	0.54	0.1	0.54	0.08	0.49	0.3	0.07	0.16	0.06	0.25	0.2
Gd	0.92	2.7	0.43	2.4	0.51	1.93	1.14	0.2	0.94	0.25	1.14	0.9
Tb												
Dy	0.57	2.3	0.36	2.3	0.34	1.8	1	0.2	0.45	0.23	0.95	0.85
Ho	0.1	0.48	0.07	0.5	0.07	0.38	0.2	0.03	0.09	0.05	0.2	0.18
Er	0.28	1.4	0.22	1.52	0.24	1.07	0.58	0.11	0.27	0.17	0.59	0.54
Tm												
Yb	0.32	1.65	0.25	1.79	0.34	1.22	0.74	0.14	0.33	0.25	0.7	0.62
Lu	0.05	0.27	0.04	0.31	0.06	0.18	0.12	0.03	0.05	0.04	0.11	0.1
ΣREE	44.7	281.5	15.58	87.76	24.99	68.67	26.99	11.58	48.54	10.08	62.04	81.21
ΣLREE	42.46	272.7	14.21	78.94	23.43	62.09	23.21	10.87	46.41	9.09	58.35	78.78
ΣHREE	2.24	8.8	1.37	8.82	1.56	6.58	3.78	0.71	2.13	0.99	3.7	3.19
LREE/HREE	18.96	30.99	10.37	8.95	15.02	9.44	6.14	15.31	21.79	9.18	14.62	7.58
Eu/Eu*	0.6	0.65	0.7	0.65	0.43	0.73	0.73	0.89	0.41	0.66	0.64	0.14
Ce/Ce*	1.44	8.36	0.94	1.06	1.02	1.05	0.11	0.8	1.01	0.95	1.67	2.37
La/Th	0.8	2.14	0.16	4.75	0.53	1.65	0.94	0.38	0.39	0.28	1.2	1.4
(La/Yb) _{cn}	19.11	6.22	10.33	7.21	12.19	8.13	9.27	16.5	22.23	6.52	11.77	5.64
(La/Sm) _{cn}	4.93	3.93	5.27	4.39	5.86	4.14	4.47	7.32	4.35	4.83	4.95	1.01
(Gd/Yb) _{cn}	2.33	1.32	1.39	1.08	1.21	1.28	1.25	1.16	2.3	0.81	1.41	0.5

Location	Downstream sector (<i>n</i> = 10)												UCC	Chondrite
Ref. code	Mb1	Mb2	Mb3	Mb4	Ma1	Ma2	Es1	Es2	Dh1	Dh2	Av	± 1σ		
La	103	8.6	8.1	3.7	97	41	7.4	4.9	3.8	9.6	28.71	39.15	30	0.237
Ce	211	17.7	15.4	7.3	195	86	14.5	9.4	7.1	18.8	58.22	79.83	64	0.613
Pr	22	2	1.76	0.86	20	9.3	1.62	1.02	0.81	2.1	6.147	8.23	7.1	0.093
Nd	77	7.6	6.4	3.1	69	33	5.6	3.6	2.8	7.6	21.57	28.57	26	0.457
Sm	12.5	1.25	1.08	0.53	10.5	5.4	0.94	0.63	0.53	1.49	3.485	4.48	4.5	0.148
Eu	1.22	0.15	0.13	0.09	0.66	0.29	0.15	0.14	0.13	0.27	0.323	0.36	0.88	0.056
Gd	8.3	0.8	0.79	0.44	7.3	3.8	0.65	0.45	0.48	1.59	2.46	3	3.8	0.199
Tb													0.64	0.036
Dy	3.6	0.56	0.41	0.28	3.3	1.56	0.38	0.31	0.52	1.83	1.28	1.27	3.5	0.246
Ho	0.56	0.1	0.08	0.05	0.58	0.3	0.08	0.06	0.12	0.43	0.24	0.21	0.8	0.055
Er	1.28	0.31	0.25	0.15	1.66	0.9	0.24	0.18	0.37	1.33	0.67	0.57	2.3	0.16
Tm													0.33	0.025
Yb	1.09	0.32	0.3	0.17	2.2	1.25	0.33	0.21	0.45	1.4	0.77	0.68	2.2	0.161
Lu	0.18	0.05	0.04	0.03	0.42	0.23	0.06	0.04	0.08	0.24	0.14	0.13	0.32	0.025
ΣREE	441.7	39.44	34.74	16.7	407.6	183	31.95	20.94	17.19	46.68	124	166		
ΣLREE	426.7	37.3	32.87	15.58	392.2	175	30.21	19.69	15.17	39.86	118.5	161		
ΣHREE	15.01	2.14	1.87	1.12	15.46	8.04	1.74	1.25	2.02	6.82	5.55	5.63		
LREE/HREE	28.44	17.4	17.54	13.92	25.37	21.76	17.36	15.75	7.53	5.84	17.09	7.06		
Eu/Eu*	0.37	0.46	0.43	0.57	0.23	0.2	0.59	0.81	0.79	0.54	0.5	0.21		
Ce/Ce*	1.07	1.03	0.99	0.99	1.07	1.07	1.01	1.02	0.98	1.01	1.03	0.04		
La/Th	9.12	1.22	0.34	0.93	8.35	4.63	0.69	0.54	0.14	1.12	2.71	3.42		
(La/Yb) _{cn}	64.19	18.26	18.34	14.79	29.95	22.28	15.23	15.85	5.74	4.66	20.93	16.87		
(La/Sm) _{cn}	5.15	4.3	4.68	4.36	5.77	4.74	4.92	4.86	4.48	4.02	4.73	0.49		
(Gd/Yb) _{cn}	6.16	2.02	2.13	2.09	2.68	2.46	1.59	1.73	0.86	0.92	2.27	1.49		

LREE = La, Ce, Pr, Nd, Sm, and Eu; HREE = Gd, Tb, Dy, Ho, Er, Tm, Yb, and Lu

$$Ce/Ce^*_{cn} = (Ce_{sample}/Ce_{chondrite}) / (La_{sample}/La_{chondrite})^{1/2} (Pr_{sample}/Pr_{chondrite})^{1/2}$$

$$Eu/Eu^*_{cn} = (Eu_{sample}/Eu_{chondrite}) / (Sm_{sample}/Sm_{chondrite})^{1/2} (Gd_{sample}/Gd_{chondrite})^{1/2}$$

$$(La/Yb)_{cn} = (La_{sample}/La_{chondrite}) / (Yb_{sample}/Yb_{chondrite})$$

$$(La/Sm)_{cn} = (La_{sample}/La_{chondrite}) / (Sm_{sample}/Sm_{chondrite})$$

$$(Gd/Yb)_{cn} = (Gd_{sample}/Gd_{chondrite}) / (Yb_{sample}/Yb_{chondrite})$$

The UCC and chondrite values are cited from Taylor and McLennan (1985) and McDonough and Sun (1995)

Av. = average, 1σ = one standard deviation, *n* = total number of samples. Subscript _{cn} refers to chondrite-normalized values. Tb and Tm data of the present study are not available

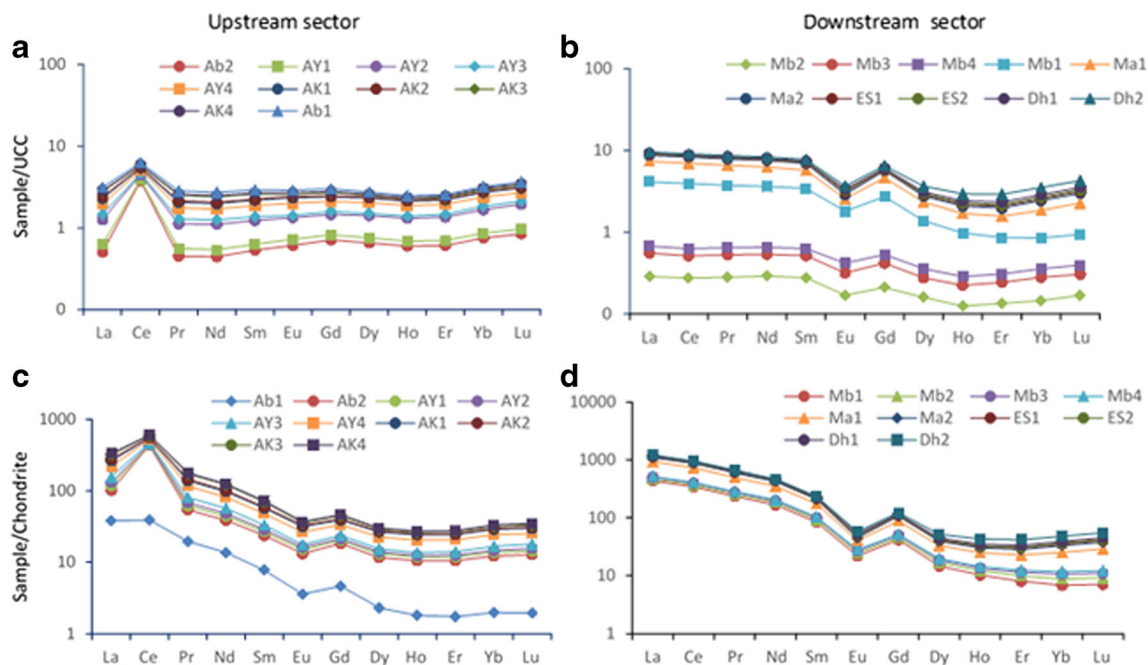


Fig. 6 UCC- and chondrite-normalized trace element patterns of the Nyong River sediments. Normalization values are from Taylor and McLennan (1985) and McDonough and Sun (1995). **a, c** Upstream sector and **b, d** downstream sector

receive contribution from both the Nyong and Ntem units. The Nyong unit experienced sedimentary cycles in Nyong intracratonic basin (2515–2535 Ma; Feybesse et al. 1998), while the Ntem unit remained always a stable craton (Tchameni et al. 2000; Shang et al. 2007).

The PIA is expressed as follows: $PIA = ((Al_2O_3 - K_2O) / (Al_2O_3 + Na_2O + CaO^* + K_2O)) * 100$ (Fedo et al. 1995), using molecular proportion. It allows the estimation of the degree of chemical weathering, excluding the influence of k-metasomatism. The PIA of unweathered plagioclase has value less than 50. This value is disposed to increase with increasing degree

of weathering (Fedo et al. 1995). The PIA of Ups and Dws samples varies from 76.7 to 98.8 and from 66.1 to 93.8, respectively (Table 5). This result is consistent with CIA values, revealing a high weathering intensity.

The CIW is expressed as follows: $CIW = [Al_2O_3 / (Al_2O_3 + CaO^* + Na_2O)] * 100$ (Harnois 1988). CIW values near 50 suggest no weathering, values varying between 60 and 80 are indicative of moderate weathering, and values > 80 indicate extreme weathering (Nesbitt and Young 1982; Selvaraj and Chen 2006). The calculated CIW values, presented in Table 5, for the Ups and Dws samples ($77.2\text{--}98.8$, 89.65 ± 7.55 and $66.95\text{--}93.98$, 82.69 ± 8.78 , respectively) indicate, overall, high degree of weathering.

The degree of weathering is linked to the mobility of cations such as Na^+ , K^+ , and Ca^{2+} during chemical weathering processes. This element mobility, for the sediments studied (i.e., weathering trend), was evaluated using $Al_2O_3\text{--}(CaO + Na_2O)\text{--}K_2O$ (A–CN–K) diagram (Nesbitt and Young 1984; Fedo et al. 1995; Fig. 8a). Theoretically, in this diagram, both parent rocks and their altered product should fall along the same linear trend. The projection of this linear trend on the plagioclase-potash feldspar joint suggests the geochemical composition and mineralogical association of the likely parental material. In the A–CN–K ternary plot, the NR sediments fall on linear trends parallel to the A–CN, far above the plagioclase-potash feldspar joint line, and close to the plagioclase side (Fig. 8a). When extended backward, the intersection of the trend lines with the feldspar joint suggest that the feldspar composition (i.e., plagioclase/k-feldspar ratio) of the sediments is similar to that of rocks such as granodiorite-tonalite

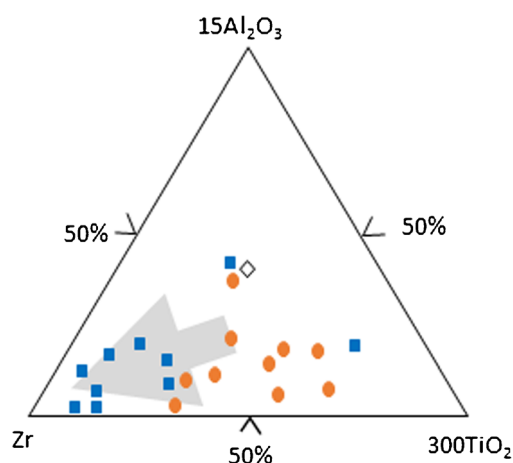


Fig. 7 Ternary plot of $Al_2O_3\text{--}TiO_2\text{--}Zr$ (after Garcia et al. 1994) for the Nyong River sediments, showing possible sorting effects and recycling

(probable source rocks present in the NR watershed). Absence or minor role of potash metasomatism is confirmed by the fact that the composition of the studied sediments fall mostly on the weathering trend of granodiorite and tonalite and do not exhibit a clear inclination toward the K_2O apex. The weathering trends of NR sediments suggest relatively non-steady state weathering conditions (Nesbitt et al. 1997; Nesbitt and Young 2004). This non-steady state weathering suggests balanced rates of chemical weathering and erosion, which produce compositionally similar sediments over a long period (Nesbitt and Young 2004), i.e., more than 500 Ma in the present case (Vicat and Pouclet 1995; Vicat et al. 1996; Feybesse et al. 1998; Pouclet et al. 2007).

The high degree of chemical weathering is also confirmed by the binary diagram ICV versus CIA (Fig. 8b) and the plot

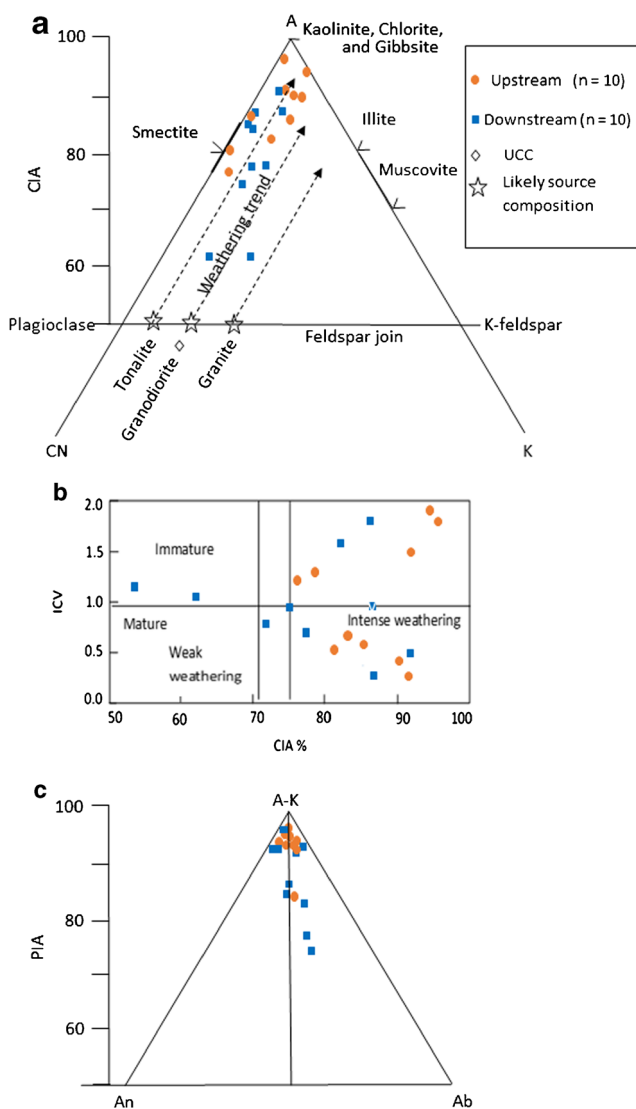


Fig. 8 a Ternary plot of A (Al_2O_3)-CN ($CaO^* + Na_2O$)-K (K_2O), b bivariate plot of ICV versus CIA, and c ternary plot of (A-K)(Al_2O_3 - K_2O)-C(CaO^*)-N(Na_2O) (Nesbitt and Young 1984; Cox et al. 1995) to infer the intensity of weathering for the Nyong River sediments

of the studied sediments in the (Al_2O_3 - K_2O)- CaO - Na_2O ((A-K)-C-N) ternary space (Fig. 8c; Nesbitt and Young 1984; Fedo et al. 1995). In the (A-K)-C-N diagram, most of the NR sediment samples plot close to the Al_2O_3 - K_2O apex, indicating, overall, intense weathering, as signified by all weathering indices.

Provenance

Major elements, such as Al_2O_3 and TiO_2 , and trace element (i.e., Hf, Th, Sc, Cr, Zr, Ni, V, and Co), including rare earth element, concentrations in clastic sediments are commonly used to infer the provenance of sedimentary clastic rocks, since they tend to mirror the source terrane composition (Garcia et al. 1994; Cullers 2000; Zhang and Gao 2015; Madhavaraju et al. 2016; Verma and Armstrong-Altrin 2016). The REE pattern and the size of Eu anomaly are also suitable to portray the source rock (Etemad-Saeed et al. 2011; Armstrong-Altrin et al. 2004, 2016). In the present study, geochemical data of the NR sediments have been presented in numerous binary diagrams, extensively used in provenance studies, to infer the composition of their source rocks (Fig. 9).

In sedimentary provenance studies, the binary diagram of Zr versus TiO_2 proposed by Hayashi et al. (1997) is frequently used (e.g., Armstrong-Altrin et al. 2012; Nguetchoua et al. 2019a, 2019b). This diagram helps to discriminate mafic rocks ($TiO_2/Zr > 200$), intermediate rocks (TiO_2/Zr ranging between 200 and 55), and felsic igneous rocks ($TiO_2/Zr < 200$). In the current study, all the samples plotted in the field of felsic igneous rocks (Fig. 9a).

Elemental ratios such as Th/Co, La/Sc, and the Th/Co versus La/Sc bivariate plot (Cullers 2002) can be used as indicators for source composition. The values of Th/Co (0.67–19.4) and La/Sc (2.50–16.3) are suggestive of felsic source, while those of Th/Co (0.04–1.4) and La/Sc (0.43–0.86) are indicative of mafic source rocks. In the current study, Th/Co and La/Sc indicate mostly felsic source rocks. This result is illustrated in the Th/Co versus La/Sc bivariate diagram, where all the samples plotted near the field of felsic (i.e., silicic) rocks (Fig. 9b). On the other hand, the major element provenance discriminant function plot of Roser and Korsch (1988) tends to indicate the presence of old and quartzose sedimentary rocks in the source region (Fig. 9c), suggesting possibly the predominance of mature polycyclic siliciclastic rocks, with subordinate contribution from first cycle basic and felsic rocks. Moreover, high Zr values (up to 5145 ppm) are indicative of high-zircon content and suggest granitic sources or recycled detrital rock sources (Carranza-Edwards et al. 2001). The ongoing analysis is based on the fact that, in the NR drainage basin basement, Vicat and Pouclet (1995), Vicat et al. (1996), Feybesse et al. (1998), and Pouclet et al. (2007) have described various metasedimentary rocks, such as metagraywakes, metaquartzites, and Banded Iron

Formation (BIF). According to Trendall (2002), BIF refers to sedimentary iron-rich layers, commonly alternating with silica-rich layers or their metamorphic equivalent.

The elevated contents of Cr (> 150 ppm), Ni (> 100 ppm), and V in clastic rocks are indicative of ultramafic rocks in the source area (Garver et al. 1996). In this study, samples from Ups and Dws have low average Cr (124.3 ± 134.4 ppm and 41.09 ± 17.79 ppm, respectively) and Ni contents (11.37 ± 13.38 ppm and 4.98 ± 2.18 ppm, respectively) indicating, overall, a felsic source areas (Table 7). It is worth noting that high contents of Cr (245–373 ppm) are recorded in samples Ab1, Ab2, and Ak1, from the Ups, indicating the presence of some mafic source rocks (e.g., gneisses, garnet gneisses, and pyroxene gneisses) in the upper reaches of NR, which flows through the Yaoundé Group, generally made up of migmatite and migmatitic gneisses. This is further supported by relative high V contents (132–340 ppm) in almost the same samples (Ab1, Ab2, Ak1, and Ay4), compared to those of other samples from both Ups and Dws (14–93 ppm).

Noteworthy too is the fact that in samples Ma1 and Ma2, relatively elevated contents of mafic components such as Ni (8.8 and 4.2 ppm, respectively), Cr (63 and 62 ppm, respectively), and V (89 and 58 ppm, respectively) are recorded, compared to their average in the Dws samples (4.98 ± 2.18 ppm, 41.09 ± 17.79 ppm, 34 ± 23.56 ppm, respectively). At points Ma1 and Ma2, the NR receives detritus from its main tributary (i.e., the So'o River), which flows on the Ntem unit,

made up of the remnant of Achaean greenstones, among other rocks (Tchameni et al. 2000; Shang et al. 2004, 2007). Hence, the relatively high contents of Cr in these samples may be due to chromite and ferromagnesian minerals (i.e., pyroxene, amphibole, and olivine), which are current minerals of greenstones. This indicates that the greenstones might have acted as a source rock of mafic detritus in the NR sediments. To sum up, the NR sediments appear to have been derived from various types of rocks, including predominantly felsic rocks and subsidiary amount of mafic and recycled detritus. The nature of the source rocks is further supported by the result of heavy mineral analysis (Table 3; Garzanti and Ando 2007). The occurrence, in the studied sediments, of heavy minerals like zircon, tourmaline, and rutile (with some subrounded grains) and the high ZTR index (> 10%), varying between 13.11 and 36.6%, indicates felsic source rocks and/or recycled source coupled with hydraulic sorting (e.g., Garzanti and Ando 2007), supporting a detrital origin. Augite, diopside, hypersthene, and rutile may suggest the contribution of mafic rocks, while garnet, kyanite, and sillimanite indicate metamorphic rocks.

The REE patterns and the size of the Eu anomaly of the NR sediments were examined in order to infer the parent rocks (e.g., Etemad-Saeed et al. 2011; Armstrong-Altrin et al. 2012, 2014). The Σ REE contents depend primarily on parent rocks, grain size, and proportion of heavy minerals (Armstrong-Altrin et al. 2018). The average Σ REE contents of Ups and

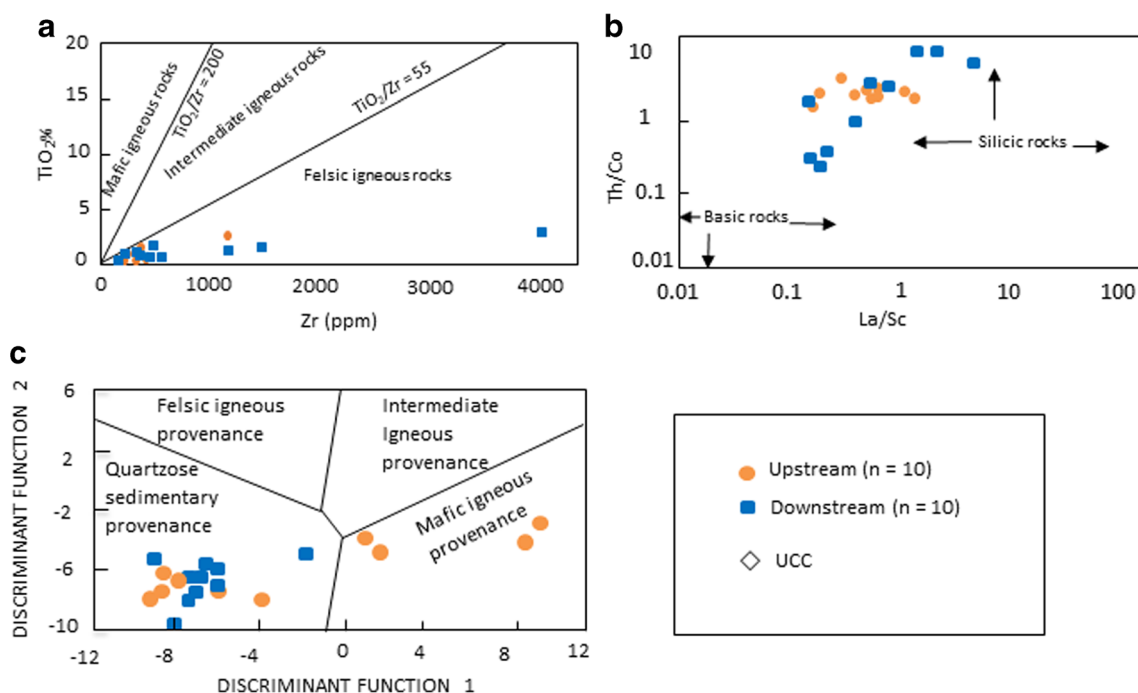


Fig. 9 Bivariate and ternary plots of the Nyong River sediments, inferring possible source rocks: **a** Zr vs. TiO_2 (after Hayashi et al. 1997), **b** Th/Co vs. La/Sc (after Cullers 2002), and **c** discriminant function plot of Roser and Korsch (1988). The discriminant functions are as follows: discriminant function 1 = $(-1.773 \cdot \text{TiO}_2) + (0.607 \cdot \text{Al}_2\text{O}_3) +$

$(0.760 \cdot \text{Fe}_2\text{O}_3) + (-1.500 \cdot \text{MgO}) + (0.616 \cdot \text{CaO}) + (0.509 \cdot \text{Na}_2\text{O}) + (-1.224 \cdot \text{K}_2\text{O}) + (-9.090)$; discriminant function 2 = $(0.445 \cdot \text{TiO}_2) + (0.070 \cdot \text{Al}_2\text{O}_3) + (0.250 \cdot \text{Fe}_2\text{O}_3) + (-1.142 \cdot \text{MgO}) + (0.438 \cdot \text{CaO}) + (1.475 \cdot \text{Na}_2\text{O}) + (-1.426 \cdot \text{K}_2\text{O}) + (-6.861)$

Dws samples are 62.04 ± 81.1 ppm and 124 ± 166 ppm, respectively, indicating probably a compositional difference between their source rocks. Note that high Σ REE are recorded in samples Mb1 (441.7 ppm), Ma1 (407.6 ppm), and Ma2 (183 ppm), compared to other samples, indicating a more mafic detritus in the middle reaches of NR. Those mafic detritus may be derived probably from the NR's main tributary, namely the So'o River which drains a part of the Ntem unit. Mafic igneous rocks commonly contain low LREE/HREE ratios and tend to show low negative or no Eu anomalies, while felsic igneous rocks generally show higher LREE/HREE ratios and display negative Eu anomalies of varied size (Cullers et al. 1987). The samples studied show high LREE/HREE ratios, excluding few samples (Ak1, Dh1, and Dh2), indicating a predominance of felsic rocks at the source area (Table 8). The UCC-normalized REE patterns for the Ups show no Eu anomalies, while in the Dws, Eu anomalies are pronounced (Fig. 6a, b). In the chondrite-normalized REE patterns for the Ups and Dws sediments, the Eu anomalies are well marked, indicating a felsic source rock and negligible contribution of mafic detritus (Fig. 6c, d; Table 8). This is consistent with the fact that most of the basement rocks of the NR drainage basin belong to the Pan-African belt. The latter consists mainly of felsic materials made up of Neoproterozoic supracrustal assemblage, variously deformed granitoids, and medium- to high-grade Neoproterozoic metamorphic rocks (gneisses, migmatitic gneisses, and migmatites). Mafic constituents from Ntem complex, i.e., remnants of greenstone belt (garnet amphibolite, metadolerite, pyroxenite, serpentinite, BIF, and ultramafic metavolcanics), seem to have not play an important role in sourcing the NR sediments. It is worth noting that the whole Archean rocks (i.e., felsic and mafic components) of the studied drainage basin noticeably contributed to the NR sediments only in the Dws, as illustrated by the binary plot of Eu/Eu* versus $(\text{Gd}/\text{Yb})_{\text{cn}}$ (Fig. 10; Taylor and McLennan 1985; McLennan and Taylor 1991). Archean crust generally has $(\text{Gd}/\text{Yb})_{\text{cn}}$

values above 2.0 in sedimentary rocks, while post Archean rocks have $(\text{Gd}/\text{Yb})_{\text{cn}}$ values varying between 1.0 and 2.0. Also, Archean crust generally has Eu/Eu* values above 0.85 in clastic rocks while post Archean rocks have pronounced Eu anomalies (Eu/Eu* values below 0.85), and this is exhibited in their detritus products (McLennan and Taylor 1991). In the Eu/Eu* versus $(\text{Gd}/\text{Yb})_{\text{cn}}$ diagram, most samples of the Ups fall below the $(\text{Gd}/\text{Yb})_{\text{cn}} = 2.0$ boundary, except two samples, which fall above this line. Almost all samples of this sector fall below the Eu/Eu* = 0.85 line, indicating, as expected that the Phanerozoic (i.e., Pan-African) rocks could be the main source rocks of the stream sediments studied. But in the Dws, five samples (over ten) fall above the $(\text{Gd}/\text{Yb})_{\text{cn}} = 2.0$ boundary and all samples of this sector fall below the Eu/Eu* = 0.85 line, indicating some contribution of the Archean rocks from the Ntem complex. The evolution of this complex may explain the quartzose sedimentary origin of the NR sediments, as revealed by the Fig. 9c.

The Ntem complex was marked by the Eburnean rifting (older than 2500 Ma), followed by the opening of the Nyong intracratonic basin, filled with detrital materials (< ca 2400 Ma; Vicat et al. 1996; Pouclet et al. 2007). These detrital materials were subsequently affected by granulite facies metamorphism at the Paleoproterozoic time. Thus, the Nyong unit is characterized by pre-orogenic sediments, explaining, in a lesser extent, the quartzose sedimentary provenance of the NR alluviums. Also, the sedimentary signature of source rocks may be linked to the Pan-African orogeny. Indeed, Pan-African events result in the opening and closure of large Proterozoic oceanic realms (Feybesse et al. 1998; Toteu et al. 2001; Kröner and Stern 2004), explaining probably the detrital provenance of the NR sediments. Furthermore, the low- to medium-grade schist of the Mbalmayo locality is thought to be of sedimentary origin (Nzenti 1998). Likewise, the garnet granulites of Yaoundé Group are considered to derive from the metamorphism of a near shore sedimentary sequence related to an old intracratonic basin. According to Nzenti (1998), this sedimentation was accompanied by alkaline volcanism and the subsequent volcanogenic greywackes were later metamorphosed to garnet granulites. The current analysis proposes that the sedimentary signature of these clastic rocks were not entirely destroyed during later tectonism and metamorphism.

The REE data of this study are compared with those of various Archean, Paleoproterozoic, and Neoproterozoic rocks outcropping within the NR drainage basin or close to the study area to infer the source rocks (Fig. 11). These rocks include calc-silicate rocks, kyanite-garnet gneisses, garnet-biotite gneisses, alkaline orthogneisses, melanosomes of migmatites, pyroxene gneisses and amphibolites, serpentinites, BIF, TTG suites, syenites, and high-k granitic rocks (Barbey et al. 1990; Ngnotue et al. 2000; Tchameni et al. 2000; Shang et al. 2004, 2007; Ganno et al. 2017, 2018; Tsoungui et al. 2019). The

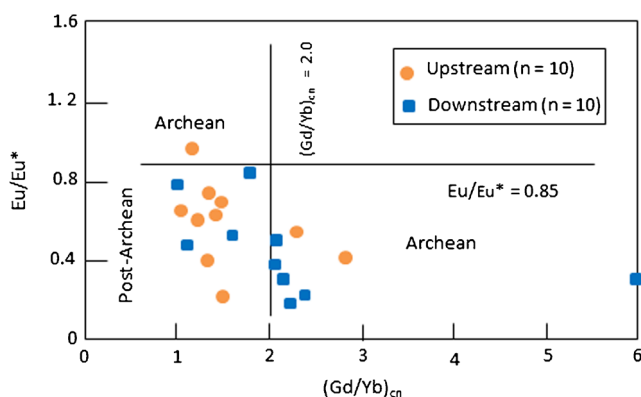


Fig. 10 Bivariate plot of Eu/Eu* vs. $(\text{Gd}/\text{Yb})_{\text{cn}}$ (after Taylor and McLennan 1985; McLennan and Taylor 1991) for the Nyong River sediments, showing a mixing of Archean and post Archean source rocks

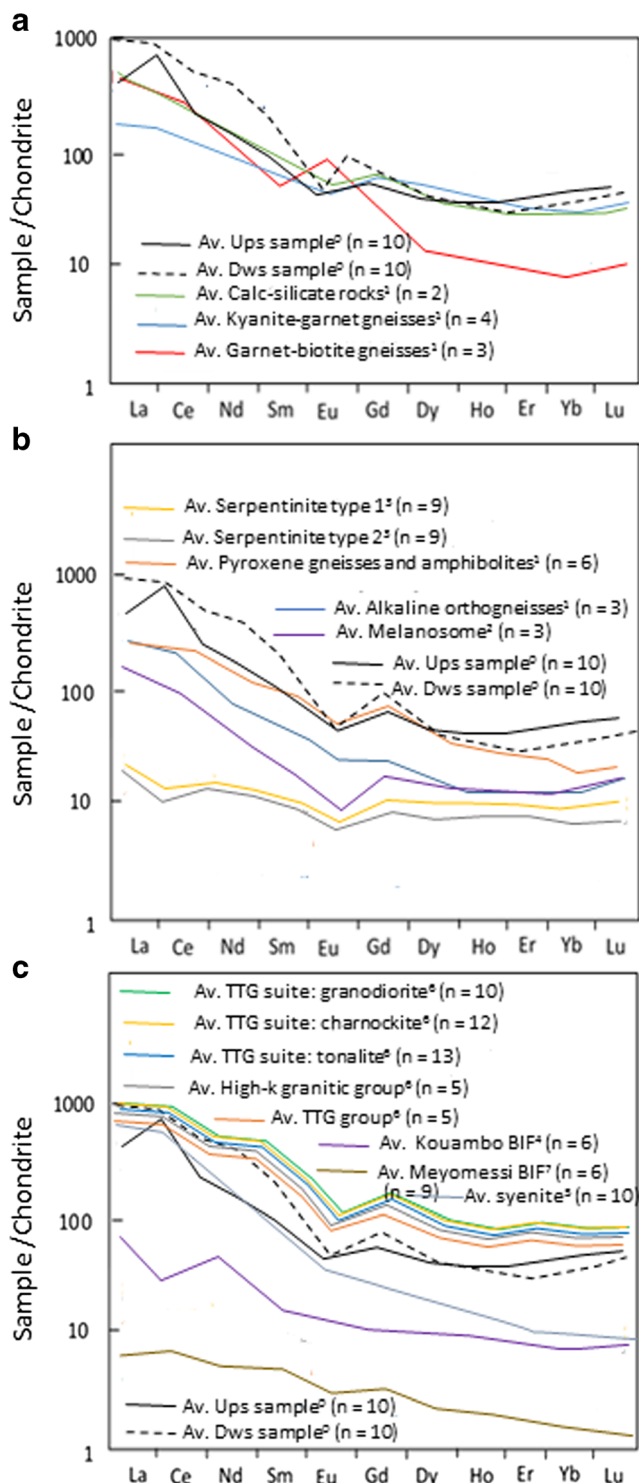


Fig. 11 Chondrite-normalized REE patterns (McDonough and Sun 1995) of the probable source rocks of the Nyong River sediments. REE data are from ⁰this study, ¹Ngnotue et al. (2000), ²Barbey et al. (1990), ³Tsougui et al. (2019), ⁴Ganno et al. (2017), ⁵Tchameni et al. (2000), ⁶Shang et al. (2004, 2007), and ⁷Ganno et al. (2018). Av. = average. Refer to Fig. 1 for the location of the source area

REE patterns and Eu anomalies of NR sediments are more or less similar to those of most of Neoproterozoic gneisses and Archean TTG suites, which suggests that these sediments were predominantly derived from the Pan-African metamorphic rocks, probably reworked from Archean and Paleoproterozoic materials. This is further supported by the Eu/Eu^* versus $(Gd/Yb)_{cn}$ binary plot (Fig. 10; Taylor and McLennan 1985; McLennan and Taylor 1991), showing a mixing of Archean and post Archean materials.

Tectonic setting

The geochemistry of clastic sediment can be used to determine the tectonic setting of the source area (Etemad-Saeed et al. 2015; Dinis and Oliveira 2016). Several discrimination diagrams using the chemical content of sediments were recently developed to determine the tectonic setting of unknown basins and that of their source terrane (Bhatia 1983; Roser and Korsch 1986; Verma and Armstrong-Altrin 2013, 2016). Among these approaches, the conventional diagrams of Bhatia (1983) and Roser and Korsch (1986) show a low success rate to infer the exact tectonic setting, according to a recent evaluation of their results (Hegde and Chavadi 2009; Armstrong-Altrin and Verma 2005). In contrast, many studies (e.g., Li et al. 2016; Maslov et al. 2016; Vosoughi Moradi et al. 2016) cautioned the good performance of the discriminant function diagrams proposed by Verma and Armstrong-Altrin et al. (2013, 2016). The latter are chosen and applied to understand the tectonic setting of the source rocks of the LR sediments. Verma and Armstrong-Altrin et al. (2013) discriminant high- and low-silica diagrams were proposed by the combination of major element concentrations to discriminate arc, rift, and collision settings. The high-silica diagram shows $(SiO_2)_{adj}$ values varying between 63 and 95%, whereas the low silica shows sediment with $(SiO_2)_{adj}$ contents varying between 35 and 63%, the subscript _{adj} referring to the fact that the chemical data were adjusted, before all calculation, to 100% on an anhydrous basis. Verma and Armstrong-Altrin et al. (2016) discrimination diagrams combine major and trace element concentrations to discriminate active (including arc and collision) and passive margin (including rift) settings. In the high silica diagram, all the samples plot into the rift field, suggesting a rift tectonic setting or a passive margin setting for their source terranes (Fig. 12a). To better ascertain the tectonic history of these source terranes, two multidimensional diagrams (i.e., one based on major elements and the other on major and trace elements) also proposed by Verma and Armstrong-Altrin et al. (2016) was applied to the studied geochemical data (Fig. 12b, c). These diagrams include the discriminant function one axis diagrams (i.e., $DF_{(A-P)M}$ and $DF_{(A-P)MT}$, where M and T stand for major and trace elements, respectively) are thought to correctly identify the active and passive margin for the far away geological past, as it is the

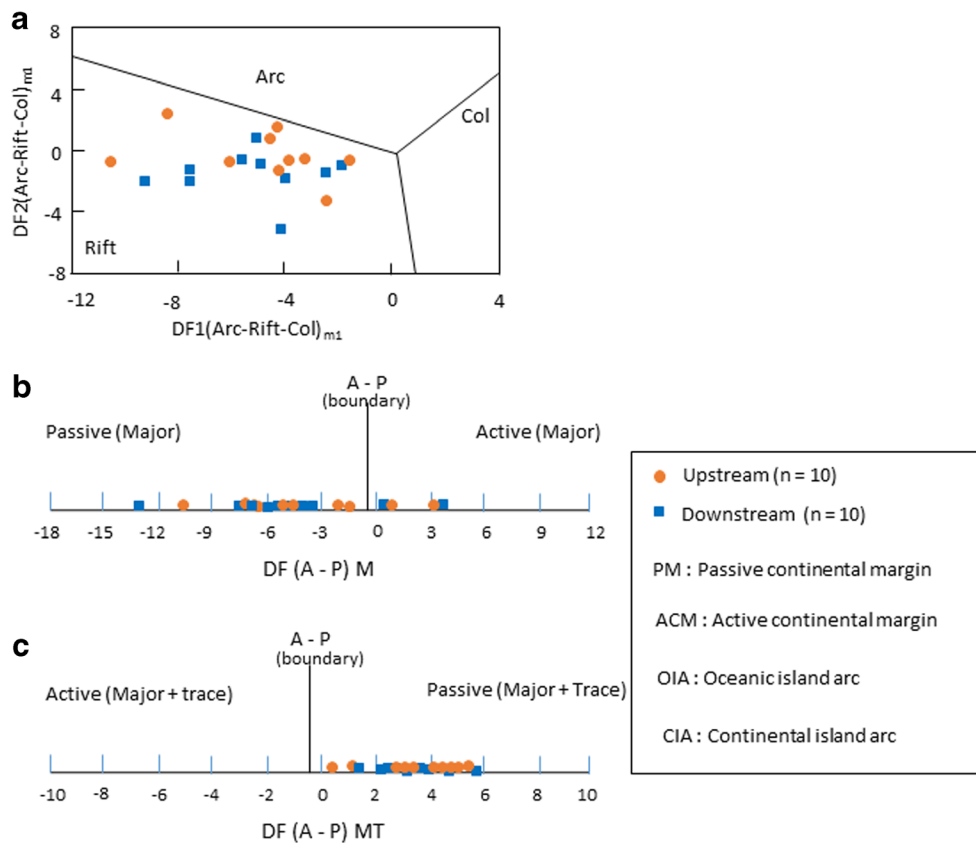


Fig. 12 Tectonic diagrams for the samples from the Nyong River sediments. **a** Discriminant function multidimensional diagram for high-silica clastic sediments (Verma and Armstrong-Altrin 2013), **b** major element (M), and **c** combined major and trace element (MT) based multidimensional discriminant function diagrams for the discrimination of active (AM) and passive (PM) margin setting (Verma and Armstrong-Altrin et al. 2016). The subscript m1 in DF1 and DF2 represents the high-silica diagram based on log_e-ratios of major elements. The discriminant function equation are as follows: $DF1 (Arc-Rift-Col)_{m1} = (-0.263 \times \ln(TiO_2/SiO_2)_{adj} + (0.604 \times \ln(Al_2O_3/SiO_2)_{adj} + (-1.725 \times \ln(Fe_2O_3t/SiO_2)_{adj} + (0.660 \times \ln(MnO/SiO_2)_{adj} + (2.191 \times \ln(MgO/SiO_2)_{adj} + (0.144 \times \ln(CaO/SiO_2)_{adj} + (-1.304 \times \ln(Na_2O/SiO_2)_{adj} + (0.054 \times \ln(K_2O/SiO_2)_{adj} + (-0.330 \times \ln(P_2O_5/SiO_2)_{adj} + 1.588$. $DF2 (Arc-Rift-Col)_{m1} = (-1.196 \times \ln(TiO_2/SiO_2)_{adj} + (1.604 \times \ln(Al_2O_3/$

$SiO_2)_{adj} + (-0.303 \times \ln(Fe_2O_3t/SiO_2)_{adj} + (0.436 \times \ln(MnO/SiO_2)_{adj} + (0.838 \times \ln(MgO/SiO_2)_{adj} + (-0.407 \times \ln(CaO/SiO_2)_{adj} + (1.021 \times \ln(Na_2O/SiO_2)_{adj} + (-1.706 \times \ln(K_2O/SiO_2)_{adj} + (-0.126 \times \ln(P_2O_5/SiO_2)_{adj} - 1.068$. The function $DF_{(A-P)M}$ is to be calculated from equation: $DF_{(A-P)M} = (3.0005 \times ilr1_{TiM}) + (-2.8243 \times ilr2_{AlM}) + (-1.0596 \times ilr3_{FeM}) + (-0.7056 \times ilr4_{MnM}) + (-0.3044 \times ilr5_{MgM}) + (0.6277 \times ilr6_{CaM}) + (-1.1838 \times ilr7_{NaM}) + (1.5915 \times ilr8_{KM}) + (0.1526 \times ilr9_{PM}) - 5.9948$. The function $DF_{(A-P)MT}$ is to be calculated from equation: $DF_{(A-P)MT} = (3.2683 \times ilr1_{TiMT}) + (5.3873 \times ilr2_{AlMT}) + (1.5546 \times ilr3_{FeMT}) + (3.2166 \times ilr4_{MnMT}) + (4.7542 \times ilr5_{MgMT}) + (2.0390 \times ilr6_{CaMT}) + (4.0490 \times ilr7_{NaMT}) + (3.1505 \times ilr8_{KM}) + (2.3688 \times ilr9_{PM}) + (2.8354 \times ilr10_{CrMT}) + (0.9011 \times ilr11_{NbMT}) + (1.9128 \times ilr12_{NiMT}) + (2.9094 \times ilr13_{VMT}) + (4.1507 \times ilr14_{YMT}) + (3.4871 \times ilr15_{ZrMT}) - 3.2088$

case for the age of the source rock investigated. In the major oxide-based plot, most of the samples fall in the passive margin setting, whereas in the major and trace elements based plot, all samples without exception plot in the field of passive margin, which also include rift setting. The passive margin is further supported by the high ZTR index. Sediments from collision orogens, magmatic arc, volcanic rifted margin, dissected rift shoulders, and cratonic shields generally have low ZTR index (< 10%), while sediments derived from passive margin display high ZTR index (Hubert 1962; Garzanti and Ando 2007). In the current study, all ZTR index are always > 20% (Table 3), indicating probably a passive margin setting.

The inferred rift and passive margin settings are consistent with the debated divergent tectonic history of the western border of the Ntem complex, which is a probable source area

of the studied deposits. It is generally argued that the Ntem complex suffered pre-Eburnean rifting older than ca. 2500 Ma (Vicat and Pouclet 1995; Vicat et al. 1996) followed by the opening of Nyong and many other ancient African intracratonic basins (i.e., Ogoue, Ayina, Ikoke-Waka and Franceville basins) between 2515 and 2435 Ma (Feybesse et al. 1998). Vicat and Pouclet (1995), Vicat et al. (1996), Feybesse et al. (1998), and Pouclet et al. (2007) suggested that the subsequent sediments were deposited in a passive margin environment on the northern edge of the Ntem complex. The metamorphism of these deposits has led to the formation of a supracrustal rock sequence (metagraywakes, BIF, sillimanite-bearing paragneisses, and amphibolites). This supracrustal sequence occurs as disrupted belts up to several kilometers in length and as xenolith in TTG (Shang et al. 2004, 2007). On

the other hand, the Pan-African rock history reveals the opening and closure of large Proterozoic oceanic basins (Toteu et al. 2001; Kröner and Stern 2004). In the study area, this statement is partly supported by the presence of metasedimentary units (kyanite-biotite-garnet gneisses, biotite-muscovite-garnet gneisses, calc-silicate rocks, and quartzite), interpreted as a continental margin sedimentary series (Ngnotue et al. 2000). The interpretation outlined above highlights the importance of the studied stream sediments in deciphering the tectonic setting and the history of the Yaoundé Group and Ntem complex, acting as source rocks, since this history is complex and yet to be fully understood. From the results obtained, it appears that the extensive deformation and metamorphism of the envisaged source rocks (Vicat and Poulet 1995; Vicat et al. 1996) did not completely obliterate the geochemical proxies of very old geodynamic events experienced by the source rocks.

Conclusion

Based on textural features, mineralogy, and geochemical compositions, the current study has documented the controls of tectonic setting in provenance, parental rock characteristics, and weathering in source regions from NR sediments and conclusions are as follows:

1. The NR sediments appear to have been derived from various types of rocks, including predominantly felsic rocks and subsidiary amount of mafic and recycled detritus. These felsic rocks belong mainly to the Pan-African Neoproterozoic supracrustal assemblage, variously deformed granitoids, and medium- to high-grade Neoproterozoic metamorphic. Mafic constituents from Ntem complex seem not to have played an important role in sourcing the NR sediments.
2. CIA, PIA, CIW, and the A–CN–K and (A–K)–C–N plots indicate that the stream sediments studied and their source areas underwent a high degree of chemical weathering. This result further suggests balanced rates of chemical weathering and erosion or indicates that chemical weathering proceeds at a higher rate than physical erosion, which is compatible with the stability of the region over a long period, i.e., more than 500 Ma.
3. The $\text{SiO}_2/\text{Al}_2\text{O}_3$, $\text{Al}_2\text{O}_3/\text{Na}_2\text{O}$, and $\text{K}_2\text{O}/\text{Na}_2\text{O}$ ratios indicate that most of the samples were texturally and compositionally mature; however, the ICV values and the DRX results reveal that some of the studied sediment samples exhibit rock forming minerals such as k-feldspars. The ternary $\text{Al}_2\text{O}_3\text{--TiO}_2\text{--Zr}$ diagram and the ZTR index suggest recycling and sorting of the sediments. The recycling signature may be linked to the tectonism, metamorphism, chemical weathering, and erosion of old Precambrian sedimentary successions.
4. The Eu/Eu* versus (Gd/Yb)_{cn} binary plot suggests that the studied stream sediments were derived from a combination of Archean and post Archean sources. This is consistent with the general geology of the region under consideration.
5. Several major and trace element discriminant function diagrams indicate rift and passive margins settings for the source terranes, which is consistent with numerous tectonic history models of the Ntem complex and Pan-African belt, which are the probable source rocks of the NR sediments. It is debated that the Ntem complex underwent pre-Eburnean rifting followed by the opening of the Nyong intracontinental basin, while the Pan-African rock history reveals the opening and perhaps the closure of large Proterozoic oceanic basins.

The results obtained further suggest that despite the extensive deformation and metamorphism of the source rocks during the Eburnean event and the Pan-African orogeny, they have preserved geochemical evidences of Archean, Paleoproterozoic, and Neoproterozoic tectonic events.

Acknowledgements This work represents part of the ongoing Ph.D. of the first author. The authors are grateful to the University of Liege (Belgium) for XRD and geochemical analysis. We are also indebted to the anonymous reviewers for their thoughtful examination of the manuscript and their constructive comments that greatly improved its final version.

Author contribution Each author has made substantial contributions to the conception or design of the work or the acquisition, analysis, or interpretation of data, or have drafted the work or substantially revised it. Field and laboratory works were performed by Yannick Steve Ngagoum Kontchipe, Aristide Nadine Sonfack, and Francis Temgo Sopié. The first draft of manuscript was written by Yannick Steve Ngagoum Kontchipe.

Funding This research was partly supported by the Department of Earth Sciences, Faculty of Sciences, University of Dschang, Cameroon, through an internal project.

Data availability All the sediment samples for major, trace, including REE, and mineralogical analysis were performed at the geology and sedimentary environment laboratories (AGEs), University of Liège, Belgium.

Code availability The XLSTAT software was used to determine the Pearson correlation coefficient.

Declarations

Ethics approval All co-authors have approved the submitted version (and any substantially modified version that involves the author's contribution to the study) and have agreed to be personally accountable for the author's own contributions.

Also, the following are worth nothing:

- Original data/materials/code upon which the submission is based are preserved following the best practices in the field so that they are retrievable for reanalysis.
- Data/materials/code presentation accurately reflects the original.

Consent to participate All authors whose names appear on the submission participated to the study; made substantial contributions to the conception of the work or the acquisition, analysis, or interpretation of data; drafted the work or revised it critically for important intellectual content; approved the version to be published; and agreed to be accountable for all aspects of the work in ensuring that questions related to the accuracy or integrity of any part of the work are appropriately investigated and resolved.

Consent for publication All authors agreed with the content and gave explicit consent to submit and that they obtained consent from the responsible authorities at the institute/organization where the work has been carried out, before the work is submitted.

Conflict of interest The authors declare no competing interests.

References

- Armstrong-Altrin JS (2009) Provenance of sands from Cazonos, Acapulco, and Bahía Kino beaches, México. *Rev Mex Cienc Geol* 26(3):764–782
- Armstrong-Altrin JS (2020) Detrital zircon U–Pb geochronology and geochemistry of the Riachuelos and Palma Sola beach sediments, Veracruz State, Gulf of Mexico: a new insight on palaeoenvironment. *J. Palaeogeogr* 9(4). <https://doi.org/10.1186/s42501-020-00075-9>
- Armstrong-Altrin JS, Verma SP (2005) Critical evaluation of six tectonic setting discrimination diagrams using geochemical data of Neogene sediments from known tectonic settings. *Sed Geol* 177:115–129
- Armstrong-Altrin JS, Lee YI, Verma SP, Ramasamy S (2004) Geochemistry of sandstones from the Upper Miocene Kudankulam Formation, southern India: implications for provenance, weathering, and tectonic setting. *J Sediment Res* 74:285–297
- Armstrong-Altrin JS, Lee YI, Kasper-Zubillaga JJ, Carranza-Edwards A, García D, Eby N, Balam V, Cruz-Ortiz NI (2012) Geochemistry of beach sands along the Western Gulf of Mexico, Mexico: implication for provenance. *Chem Erde* 72:345–362
- Armstrong-Altrin JS, Nagarajan R, Madhavaraju J, Rosales-Hoz L, Lee YI, Balam V, Cruz-Martinez A, Avila-Ramirez G (2013) Geochemistry of Jurassic and Upper Cretaceous shales from the Molango Region, Hidalgo, eastern Mexico: implications for source-area weathering, provenance, and tectonic setting. *CR Geosci* 345(4):185–202. <https://doi.org/10.1016/j.crt.2013.03.004>
- Armstrong-Altrin JS, Nagarajan R, Balam V, Natalhy-Pineda O (2015) Petrography and geochemistry of sands from the Chachalacas and Veracruz beach areas, western Gulf of Mexico, Mexico: constraints on provenance and tectonic setting. *J South Am Earth Sci* 64:199–216
- Armstrong-Altrin JS, Lee YI, Kasper-Zubillaga JJ, Trejo-Ramírez E (2016) Mineralogy and geochemistry of sands along the Manzanillo and El Carrizal beach areas, southern Mexico: implications for palaeoweathering, provenance and tectonic setting. *Geol J*. <https://doi.org/10.1002/gj.2792>
- Armstrong-Altrin JS, Ramos-Vázquez MA, Zavala-León AC, Montiel-García PC (2018) Provenance discrimination between Atasta and Alvarado beach sands, western Gulf of Mexico, Mexico: constraints from detrital zircon chemistry and U–Pb geochronology. *Geol J*:1–25. <https://doi.org/10.1002/gj.3122>
- Armstrong-Altrin JS, Alfonso V, Botello AV, Villanueva SF, Soto LA (2019) Geochemistry of surface sediments from the northwestern Gulf of Mexico: implications for provenance and heavy metal contamination. *Geol Q* 63(3):522–538
- Armstrong-Altrin JS, Ramos-Vázquez MA, Hermenegildo-Ruiz NY, Madhavaraju J (2020) Microtexture and U–Pb geochronology of detrital zircon grains in the Chachalacas beach, Veracruz State, Gulf of Mexico *Geol J*:1–21. <https://doi.org/10.1002/gj.3984>
- Bakkiraj D, Nagendra R, Nagarajan R, Armstrong-Altrin JS (2010) Geochemistry of sandstones from the upper Cretaceous Sillakkudi Formation, Cauvery Basin, southern India: implication for provenance. *J Geol Soc India* 76:453–467
- Barbey P, Macaudière J, Nzenti JP (1990) High-pressure melting of metapelites: evidence from the migmatites of Yaoundé. *J Petrol* 31(2):401–427
- Bhatia MR (1983) Plate tectonics and geochemical composition of sandstone. *J Geol* 91:611–627
- Bhatia MR, Crook KAW (1986) Trace element characteristics of graywackes and tectonic discrimination of sedimentary basins. *Contrib Mineral Petrol* 92:181–193
- Carranza-Edwards A, Centeno-García L, Rosales-Hoz L, Lozano-Santa Cruz R (2001) Provenance of beach gray sands from western Mexico. *J South Am Earth Sci* 14:291–301
- Carroll D (1970) Clay minerals: a guide to their x-ray identification. *Geol Soc Am* 80
- Chen M, Sun M, Cai K, Buslov MM, Zhao G, Rubanova ES (2014) Geochemical study of the Cambrian-Ordovician meta-sedimentary rocks from the northern Altai-Mongolian terrane northwestern Central Asian Orogenic Belt: implications on the provenance and tectonic setting. *J Asian Earth Sci* 96:69–83
- Cox R, Low DR, Culler RL (1995) The influence of sediment recycling and basement composition on evolution of mudrock chemistry in the southwestern United States. *Geochim Cosmochim Acta* 59:219–2940
- Cullers RL (2000) The geochemistry of shales, siltstones, and sandstones of Pennsylvanian-Permian age, Colorado, USA: implications for provenance and metamorphic studies. *Lithos* 51:181–203
- Cullers RL (2002) Implications of elemental of elemental concentrations for provenance, redox conditions, and metamorphic studies of shales and limestones near Pueblo, CO, USA. *Chem Geol* 191:305–327
- Cullers RL, Barrett T, Carlson R, Robinson B (1987) Rare earth element and mineralogic changes in Holocene soil and stream sediment: a case study in the Wet Mountains, Colorado, U.S.A. *Chem Geol* 63:275–297
- Cullers RL, Basu A, Suttner LJ (1988) Geochemical signature of provenance in sand-mixed material in soils and stream sediments near the Tobacco Root batholith, Montana, U.S.A. *Chem Geol* 70:335–348
- Dinis P, Oliveira A (2016) Provenance of Pliocene clay deposits from the Iberian Atlantic Margin and compositional changes during recycling. *Sed Geol* 336:171–182
- Ekoka Bessa AZ, Nguetchoua G, Ndjigui PD (2018) Mineralogy and geochemistry of sediments from Simbock Lake, Yaoundé area (southern Cameroon): provenance and environmental implications. *Arab J Geosci* 11(22):710. <https://doi.org/10.1007/s12517-018-4061-x>
- Ekoka Bessa AZ, Nguetchoua G, Kwewouo Janpou A, El-Amier YA, Njike Njome Mbella Nguetnga OA, Kankeu Kayou UR, Bisse SB, Ngo Mapuna EC, Armstrong-Altrin JS (2020) Heavy metal contamination and its ecological risks in the beach sediments along the Atlantic Ocean (Limbe coastal fringes, Cameroon). *Earth Syst Environ*. <https://doi.org/10.1007/s41748-020-00167-5>
- Etemad-Saeed N, Hosseini-Barzi M, Armstrong-Altrin JS (2011) Petrography and geochemistry of clastic sedimentary rocks as

- evidence for provenance of the Lower Cambrian Lalun Formation, Posht-e-badam block, central Iran. *J Afr Earth Sci* 61:142–159
- Etamad-Saeed N, Hosseini-Barzi M, Adabi MH, Sadeghi A, Houshmandzadeh A (2015) Provenance of Neoproterozoic sedimentary basement of northern Iran, Kahar Formation. *J Afr Earth Sci* 111:54–75
- Fedo CM, Nesbitt HW, Young GM (1995) Unravelling the effects of potassium metasomatism in sedimentary rocks and paleosols, with implications for paleoweathering conditions and provenance. *Geology* 23:921–924
- Feybesse JL, Johan V, Triboulet C, Guerrot C, Mayaga-Mokolo F, Bouchot V, Eko N'Dong J (1998) The West Central African belt: a model of 2.5–2.0 Ga accretion and two-phase orogenic evolution. *Precambrian Res* 87:161–216
- Folk RL (1980) *Petrology of sedimentary rocks*. Hemphill Publishing, Austin, Texas
- Fu XG, Wang J, Zeng YH, Tan FW, He JI (2011) Geochemistry and origin of rare earth elements (REEs) in the Shengli River oil shale, northern Tibet, China. *Chem Erde* 71(1):21–30
- Gallala W, Gaid ME, Montacer M (2009) Detrital mode, mineralogy and geochemistry of the Sidi Aïch Formation (Early Cretaceous) in central and southwestern Tunisia: implication for provenance, tectonic setting and paleoenvironment. *J Afr Earth Sci* 53:159–170
- Ganno S, Njiosseu Tanko EL, Kouankap Nono GD, Djoukouo Soh A, Moudio C, Ngnotué T, Nzenti JP (2017) A mixed seawater and hydrothermal origin of superior-type banded iron formation (BIF)-hosted Kouambo iron deposit, Palaeoproterozoic Nyong series, Southwestern Cameroon: constraints from petrography and geochemistry. *Ore Geol Rev* 80:860–875
- Ganno S, Tsozué D, Kouankap Nono D, Tchouatcha MS, Ngnotué T, Gamgne Takam R, Nzenti JP (2018) Geochemical constraints on the origin of Banded Iron Formation-hosted iron ore from the Archean Ntem complex (Congo craton) in the Meyomessi area, southern Cameroon. *Resour Geol*. <https://doi.org/10.1111/rge.12172>
- García D, Fontelles M, Moutte J (1994) Sedimentary fractionations between Al, Ti, and Zr, and the genesis of strongly peraluminous granites. *J Geol* 102:411–422
- Garver JI, Royce PR, Smick TA (1996) Chromium and nickel in shale of the Taconic foreland: a case study for the provenance of fine-grained sediments with an ultramafic source. *J Sediment Res* 100:100–106
- Garzanti E, Ando S (2007) Heavy mineral concentration in modern sands: implications for provenance interpretation. *Dev Sedimentology* 58:517–545
- Gromet LP, Dymek RF, Hasky LA, Korotev RL (1984) The “North American shale composite”: its compilation, major and trace element characteristics. *Geochim Cosmochim Acta* 48:2469–2482
- Harnois L (1988) The CIW index: a new chemical index of weathering. *Sed Geol* 55:319–322
- Hayashi KI, Fujisawa H, Holland HD, Ohmoto H (1997) Geochemistry of ~ 1.9 Ga sedimentary rocks from northeastern Labrador, Canada. *Geochim Cosmochim Acta* 61:4115–4137
- Hegde VS, Chavadi VC (2009) Geochemistry of Late Archaean metagreywackes from the western Dharwar Craton, south India: implications for provenance and nature of the Late Archaean crust. *Gondwana Res* 15(2):178–187
- Hernández-Hinojosa V, Montiel-García PC, Armstrong-Altrin JS, Nagarajan R, Kasper-Zubillaga JJ (2018) Textural and geochemical characteristics of beach sands along the western Gulf of Mexico, Mexico. *Carpathian J Earth Environ Sci* 13(1):161–174
- Herron MM (1988) Geochemical classification of terrigenous sands and shales from core or log data. *J Sediment Petrol* 58:820–829
- Hubert JF (1962) A zircon-tourmaline–rutile maturity index and the interdependence of the composition of heavy mineral assemblages with the gross composition and texture of sandstone. *J Sediment Petrol* 32:440–450
- Jarvis K (1990) A critical evaluation of two sample preparation techniques for low-level determination of some geologically incompatible elements by inductively coupled plasma-mass spectrometry. *Chem Geol* 83:89–103
- Kassi AM, Grigsby JD, Khan AS, Kasi AK (2015) Sandstone petrology and geochemistry of the Oligocene-Early Miocene Panjgur Formation, Makran accretionary wedge, southwest Pakistan: implications for provenance, weathering and tectonic setting. *J Asian Earth Sci* 105:192–207
- Khan T, Khan MS (2015) Clastic rock geochemistry of Punagarh basin, trans-Aravalli region, NW Indian shield: implications for paleoweathering, provenance, and tectonic setting. *Arabian J Geosci* 8:3621–3644
- Kröner A, Stern RJ (2004) *Pan-African orogeny, vol 1*. Elsevier, Amsterdam, pp 1–12
- Krumm S (1996) WINFIT 1.2: version of November 1996 (The Erlangen geological and mineralogical software collection) of ‘WINFIT’ 1.0: a public domain program for interactive profile-analysis under WINDOWS. In: Conference on Clay Mineralogy and Petrology, vol 38. Acta Universitatis Carolinae Geologica, Praha, pp 253–261
- Li B, Zhuang X, Liu X, Wu C, Zhou J, Ma X (2016) Mineralogical and geochemical composition of Middle Permian Lucaogou Formation in the southern Junggar Basin, China: implications for paleoenvironment, provenance, and tectonic setting. *Arab J Geosci* 9:174. <https://doi.org/10.1007/s12517-015-2154-3>
- Madhavaraju J (2015) Geochemistry of Late Cretaceous sedimentary rocks of the Cauvery Basin, south India: constraints on paleoweathering, provenance, and end Cretaceous environment. *Chemostratigraphy*:185–214. <https://doi.org/10.1016/B978-0-12-419968-2.00008-X>
- Madhavaraju J, Ramírez-Montoya E, Monreal R, González-León CM, Pi-Puig T, Espinoza-Maldonado IG, Grijalva-Noriega FJ (2016) Paleoclimate, paleoweathering and paleoredox conditions of Lower Cretaceous shales from the Mural Limestone, Tuape section, northern Sonora, Mexico: constraints from clay mineralogy and geochemistry. *Rev Mex Cien Geol* 33(1):34–48
- Maslov JM, Podkovyrov VN, Mizens GA, Noshkin AD, Fazliakhmetov AM, Malinovsky AI, Khudoley AK, Kovota LN, Kuptsova AV, Gareev EZ, Zainullin RI (2016) Tectonic setting discrimination diagrams for terrigenous rocks: a comparison. *Geochem Int* 54(7): 569–583
- Mbale Ngama E, Sababa E, Bayiga EC, Ekoa Bessa AZ, Ndjigui P-D, Bilong P (2019) Mineralogical and geochemical characterization of the unconsolidated sands from the Mefou River terrace, Yaoundé area, Southern Cameroon. *J Afr Earth Sci* 159:103570
- McDonough WF, Sun S-S (1995) The composition of the Earth. *Chem Geol* 120:223–253
- McLennan SM (1989) Rare earth elements in sedimentary rocks: influences of provenance and sedimentary processes. *Rev Mineral* 21: 169–200
- McLennan SM (1993) Weathering and global denudation. *J Geol* 101: 295–303
- McLennan SM, Taylor SR (1991) Sedimentary rocks and crustal evolution: tectonic setting and secular trends. *J Geol* 99:1–2
- Miounnde AP, Mbouï FAK, Kue PRM, Kabir SA, Bessong M, Liqiang Z (2019) Sedimentological studies of alluvium deposits along Ngovayang-Bipindi of Lokoundje River, Southwestern Cameroon. *Int J Geosci* 10:119–139
- Mongelli G, Critelli S, Perri F, Sonnino M, Perrone V (2006) Sedimentary recycling, provenance and paleoweathering from chemistry and mineralogy of Mesozoic continental redbed mudrocks, Peloritani Mountains, Southern Italy. *Geochem J* 40: 197–209
- Nagarajan R, Armstrong-Altrin JS, Nagendra R, Madhavaraju J, Moutte J (2007) Petrography and geochemistry of terrigenous sedimentary rocks in the Neoproterozoic Rabanpalli formation, Bhima Basin,

- northern Karnataka, Southern India: implications for paleoweathering condition, provenance, and source rocks composition. *J Geol Soc India* 70:297–312
- Nascimento DR, Sawakuchi AO, Guedes CCF, Giannini PCF, Grohmann CH, Ferreira MP (2015) Provenance of sands from the confluence of the Amazon and Madeira rivers based on detrital heavy minerals and luminescence of quartz and feldspar. *Sed Geol* 316:1–2
- Ndjigui P-D, Ebah Abeng SA, Ekomané E, Nzeukou NA, Ngo Mandeng FS, Lindjeck MM (2015) Mineralogy and geochemistry of pseudogley soils and recent alluvial clastic sediments in the Ngog-Lituba region, Southern Cameroon: an implication to their genesis. *J Afr Earth Sci* 108:1–14
- Ndjigui P-D, Onana VL, Sababa E, Bayiga EC (2018) Mineralogy and geochemistry of the Lokoundje alluvial clays from the Kribi deposits, Cameroonian Atlantic coast: implications for their origin and depositional environment. *J Afr Earth Sci* 143:102–117
- Nédelec A, Macaudière J, Nzenti JP, Barbey P (1986) Evolution métamorphique et structurale des schistes de Mbalmayo (Cameroun). Implications pour la structure de la zone mobile panafricaine d'Afrique centrale, au contact du craton du Congo. *CR Acad Sci Paris* 303:75–80
- Nesbitt HW, Young GM (1982) Early Proterozoic climates and plate motions inferred from major element chemistry of lutites. *Nature* 299:715–717
- Nesbitt HW, Young GM (1984) Prediction of some weathering trends of plutonic and volcanic rocks based on thermodynamic and kinetic consideration. *Geochim Cosmochim Acta* 48:1523–1534
- Nesbitt HW, Young GM (2004) Ancient climatic and tectonic settings inferred from paleosols developed on igneous rocks. In: Eriksson PG, Alternan W, Nelson DR, Mueller WU, Catuneanu O (eds) *The Precambrian earth: tempos and events*. Elsevier, Amsterdam, pp 482–493
- Nesbitt HW, Fedo CM, Young GM (1997) Quartz and feldspar stability, steady and non-steady-state weathering, and petrogenesis of siliciclastic sands and muds. *J Geol* 105(2):173–192
- Ngnotue T, Nzenti JP, Tchoua FM (2000) The Ntui-Betamba high-grade gneisses: a northward extension of Pan-African Yaoundé gneisses in Cameroon. *J Afr Earth Sci* 2:369–381
- Ngueutchoua G, Ekoua Bessa AZ, Eyong TJ, Demanou ZD, Baba Djaoro H, Tchami NL (2019a) Geochemistry of cretaceous fine-grained siliciclastic rocks from Upper Mundek and Logbadjeck formations, Douala sub-basin, SW Cameroon: implications for weathering intensity, provenance, paleoclimate, redox condition, and tectonic setting. *J Afr Earth Sci* 152:215–236
- Ngueutchoua G, Eyong TJ, Ekoua Bessa AZ, Azanji Agheenwi ZB, Emame Maschouer A, Sobdjour Kemteu C, Lontchi Dzoti Y, Hamadou T, Ongbassouek Baboule B-M, Kenfack Nguemo GR (2019b) Provenance and depositional history of Mesozoic sediments from the Mamfe basin and Douala sub-basin (SW Cameroon) unraveled by geochemical analysis. *J Afr Earth Sci* 158:103550. <https://doi.org/10.1016/j.jafrearsci.2019.103550>
- Nzenti JP (1998) Neoproterozoic alkaline meta-igneous rocks from the Pan-African North Equatorial fold belt (Yaoundé, Cameroon): biotites and magnetite rich pyroxenites. *J Afr Earth Sci* 26:37–47
- Nzenti JP, Barbey P, Jegouzo P, Moreau C (1984) Un nouvel exemple de ceinture granulitique dans une chaîne proterozoïque de collision: les migmatites de Yaoundé au Cameroun. *CR Acad Sci Paris* 299: 1197–1199
- Nzenti JP, Barbey P, Macaudière J, Soba D (1988) Origin and evolution of late Precambrian high-grade Yaoundé gneisses (Cameroon). *Precambrian Res* 38:91–109
- Olivry JC (1986) Fleuves et rivières du Cameroun. Collection Monographies Hydrologiques, ORSTOM, No. 9, Paris p 733
- Penaye J, Toteu SF, Van Schmus WR, Nzenti JP (1993) Données géochronologiques préliminaires (U-Pb et Sm-Nd) sur la série de Yaoundé: âge du métamorphisme granulitique de la zone mobile panafricaine à proximité du craton du Congo. *CR Acad Sci Paris* 317:789–797
- Penaye J, Toteu SF, Tchameni R, Van Schmus WR, Tchakounte J, Ganwa A, Minyem D, Nsifa EN (2004) The 2.1 Ga West central African Belt in Cameroon: extension and evolution. *J Afr Earth Sci* 39:159–164
- Poulet A, Tchameni R, Mezger K, Vidal M, Nsifa NE, Shang CK (2007) Archean crustal accretion at the northern border of the Congo craton (South Cameroon), the charnockite-TTG link. *Bull Soc Geol Fr* 178:331–342
- Ramos-Vázquez MA, Armstrong-Altrin JS (2019) Sediment chemistry and detrital zircon record in the Bosque and Paseo del Mar coastal areas from the southwestern Gulf of Mexico. *Mar Petrol Geol* 110: 650–675
- Roddaz M, Viers J, Brusset S, Baby P, Boucayrand C, Hérail G (2006) Controls on weathering and provenance in the Amazonian foreland basin: insights from major and trace element geochemistry of Neogene Amazonian sediments. *Chem Geol* 226:31–65
- Roser BP, Korsch RJ (1986) Determination of tectonic setting of sandstone-mudstone suites using Si₂O content and K₂O/Na₂O ratio. *J Geol* 94:635–650
- Roser BP, Korsch RJ (1988) Provenance signature of sandstone-mudstone suites determined using discrimination function analysis of major-element data. *Chem Geol* 67:119–139
- Ross DJK, Bustin RM (2009) Investigating the use of sedimentary geochemical proxies for paleoenvironment interpretation of thermally mature organic-rich strata: examples from the Devonian-Mississippian shales, western Canadian sedimentary basin. *Chem Geol* 220:1–19
- Roy PD, Caballero M, Lozano R, Smykatz-Kloss W (2008) Geochemistry of Late Quaternary sediments from Tecocomulco Lake, central Mexico: implication to chemical weathering and provenance. *Chem Erde* 68:383–393
- Sabaou N, Ait-Salem H, Zazoum RS (2009) Chemostratigraphy, tectonic setting and provenance of the Cambro-Ordovician clastic deposits of the subsurface Algerian Sahara. *J Afr Earth Sci* 55:158–174
- Saha S, Banerjee S, Burley SD, Ghosh A, Saraswati PK (2010) The influence of flood basaltic source terrains on the efficiency of tectonic setting discrimination diagrams: an example from the Gulf of Khambhat, western India. *Sed Geol* (1–2):1–13
- Selvaraj K, Chen C-TA (2006) Moderate chemical weathering of subtropical Taiwan: constraints from solid-phase geochemistry of sediments and sedimentary rocks. *J Geol* 114:101–116
- Shang CK, Satir M, Siebel W, Nsifa EN, Taubald H, Liégeois J-P, Tchoua FM (2004) TTG magmatism in the Congo craton: a view from major and trace element geochemistry, Rb-Sr and Sm-Nd systematics: case of the Sangmelima region, Ntem complex, southern Cameroon. *J Afr Earth Sci* 40:61–79
- Shang CK, Satir M, Nsifa EN, Liégeois J-P, Siebel W, Taubald H (2007) Archean high-K granitoids produced by remelting of earlier Tonalite-Trondhjemite-Granodiorite (TTG) in the Sangmelima region of the Ntem complex of the Congo craton, southern Cameroon. *Int J Earth Sci* 96:817–841
- Shao JQ, Yang SY (2012) Does chemical index of alteration (CIA) reflect silicate weathering and monsoonal climate in the Changjiang River basin? *Chin Sci Bull* 57:1178–1187
- Taylor SR, McLennan SM (1985) *The continental crust: its composition and evolution*. Blackwell Scientific, Oxford
- Tchameni R, Mezger K, Nsifa NE, Poulet A (2000) Late Archean crustal evolution in the Congo craton: evidence from the K-rich granitoids of the Ntem Complex, southern Cameroon. *J Afr Earth Sci* 30:133–147
- Toteu SF, Bertrand JM, Penaye J, Macaudière J, Angoua S, Barbey P (1991) Cameroon: a tectonic keystone in the Pan-African network. In Lewry JF, Stauffer MR (ed) *The Early Proterozoic Trans-Hudson Orogen of North America*. Geosci Can Special paper 37:483–496

- Toteu SF, Van Schmus WR, Penaye J, Michard A (2001) New U-Pb and Sm-Nd data from north-central Cameroon and its bearing on the Pre-Pan-African history of central Africa. *Precambrian Res* 108:45–73
- Toteu SF, Penaye J, Poudjom Djomani YH (2004) Geodynamic evolution of the Pan-African belt in Central Africa with special reference to Cameroon. *Can J Earth Sci* 41:73–85
- Trendall AF (2002) The significance of iron formation, in Precambrian stratigraphic record. *Sedimentol Spec Publ* 33:33–66
- Tsoungui PNE, Ganno S, Njiosseu Tanko EL, Mbongue JLN, Woguia BK, Tamehe L, Takodjou Wambo JD, Nzenti JP (2019) Geochemical constraints on the origin and tectonic setting of the serpentized peridotites from the Paleoproterozoic Nyong series, Eseka area, SW Cameroon. *Acta Geochim*. <https://doi.org/10.1007/s11631-019-00368-4>
- Újvári G, Varga A, Balogh-Brunstad ZS (2008) Origin, weathering, and geochemical composition of loess in southwestern Hungary. *Quat Res* 69:421–437
- Verma SP, Armstrong-Altrin JS (2013) New multi-dimensional diagrams for tectonic discrimination of siliciclastic sediments and their application to Pre-Cambrian basins. *Chem Geol* 355:117–180
- Verma SP, Armstrong-Altrin JS (2016) Geochemical discrimination of siliciclastic sediments from active and passive margin settings. *Sed Geol* 332:1–12
- Vicat JP, Pouclet A (1995) Nature du magmatisme lié à une extension pré-panafricaine : les dolérites des bassins de Comba et de Sembé-Ouessou. *Bull Soc Geol Fr* 166(4):355–364
- Vicat JP, Léger JM, Nsifa NE, Piguet P, Zenith JP, Tchameni R, Pouclet A (1996) Distinction au sein du craton congolais du Sud-Ouest du Cameroun de deux épisodes doléritiques initiant les cycles orogéniques éburnéen (paleoproterozoïque) et panafricain (Néoproterozoïque). *CR Acad Sci Paris* 323:575–582
- Vosoughi Moradi A, Sari A, Akkaya P (2016) Geochemistry of the Miocene oil shale (Hançilli Formation) in the Çankiri-Çorum Basin, Central Turkey: implications for paleoclimate conditions, source-area weathering, provenance, and tectonic setting. *Sed Geol* 78:136–150
- Wang W, Zhou M-F (2013) Petrological and geochemical constraints on provenance, paleoweathering, and tectonic setting of the Neoproterozoic sedimentary basin in the eastern Jiangnan Orogen, South China. *J Sediment Res* 83:975–994
- Xie Y, Chi Y (2016) Geochemical investigation of dry- and wet-deposited dust during the same dust-storm event in Harbin, China: constraint on provenance and implications for formation of Aeolian loess. *J Asian Earth Sci* 120:43–61
- Zhang Y, Gao X (2015) Rare earth elements in surface sediments of a marine coast under heavy anthropogenic influence: the Bohai Bay, China. *Estuar Coast Shelf Sci* 164:86–93